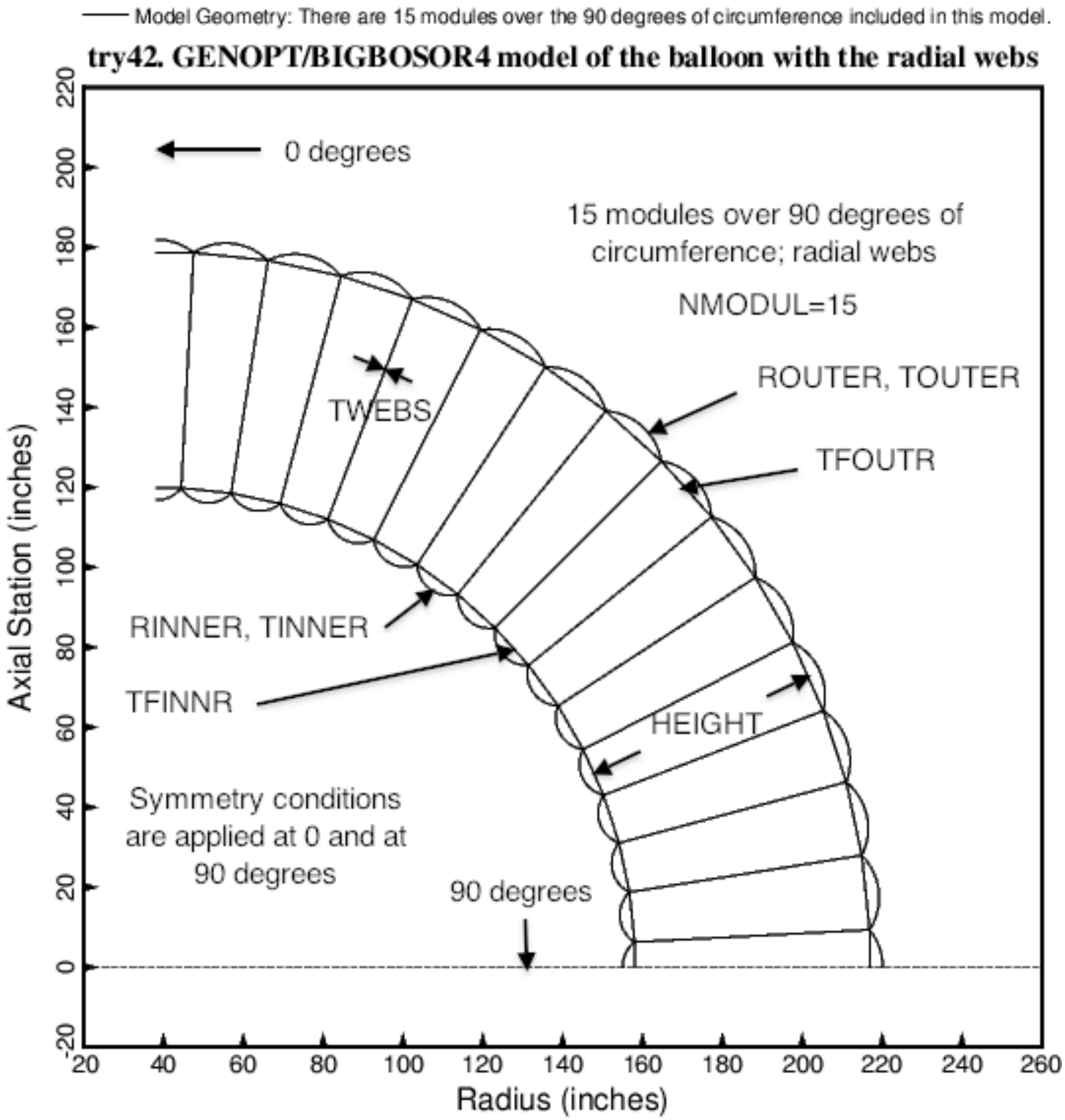

Fig. 1 Cross section of the double wall of the cylindrical vacuum chamber with **radial webs**. The radius to the inner wall is RADIUS, which is not a decision variable. The decision variable candidates are the distance between the inner and outer walls, HEIGHT, the two radii of curvature, RINNER and ROUTER, and the five thicknesses, TINNER, TOUTER, TFINNR, TFOUTR, and TWEBS. (TWEBS is misspelled: it should be TFWEBS.) The pressure inside the inner wall is PINNER; the pressure outside the outer wall is POUTER; The pressure between the inner and outer walls is PMIDDL. PMIDDL > POUTER > PINNER. Buckling of and stress in this configuration is computed with use of the BIGBOSOR4 computer program. The wall is optimized (minimum weight) with the use of the system of computer programs called "**GENOPT/BIGBOSOR4**" [2, 6, and 8 – 11].

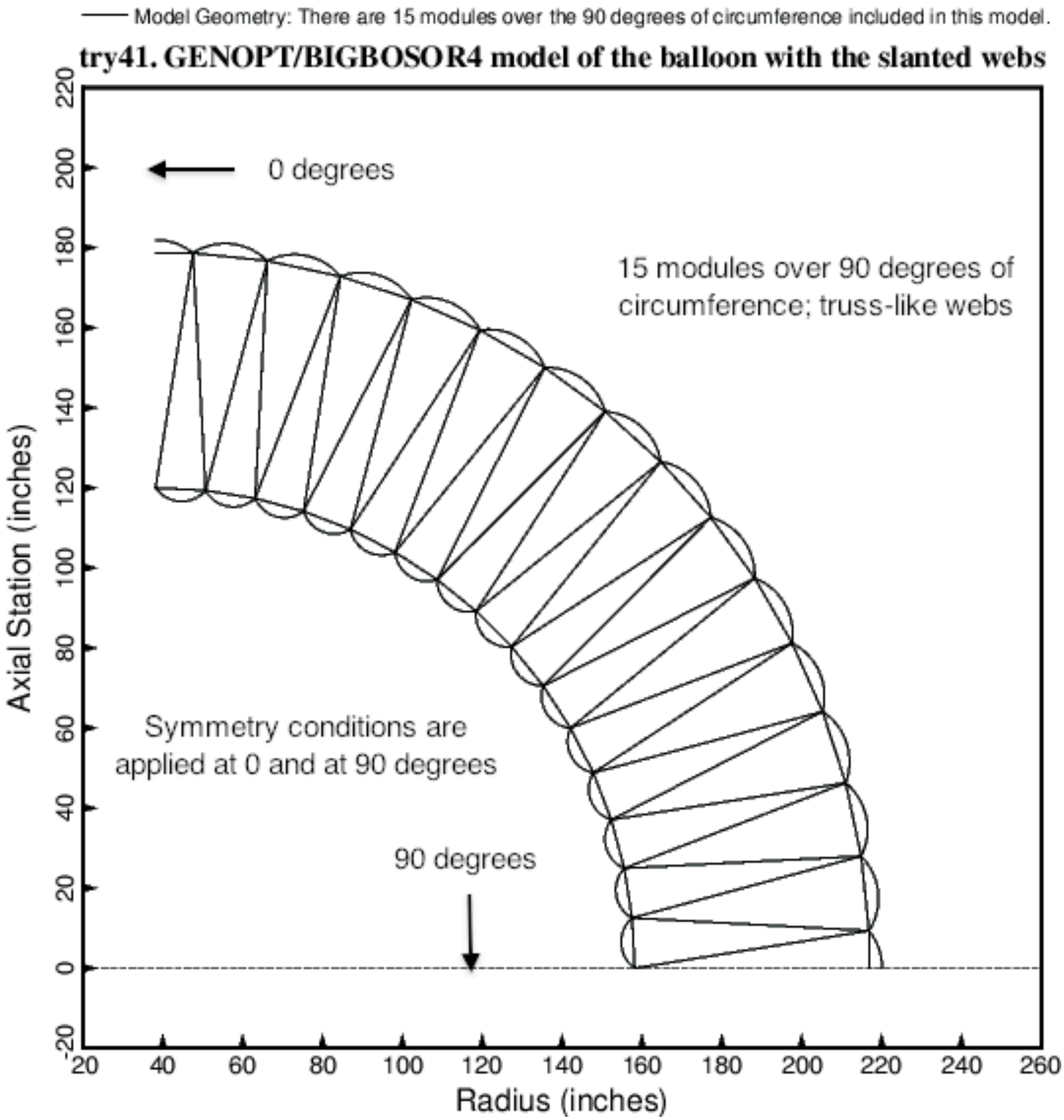

Fig. 2 Cross section of the double wall of the cylindrical vacuum chamber with **truss-like (slanted) webs**. The pressure inside the inner wall is PINNER; the pressure outside the outer wall is POUTER; The pressure between the inner and outer walls is PMIDDL. PMIDDL > POUTER > PINNER. Buckling of and stress in this configuration is computed with use of the BIGBOSOR4 computer program. The wall is optimized (minimum weight) with the use of the system of computer programs called "**GENOPT/BIGBOSOR4**" [2, 6, and 8 – 11].

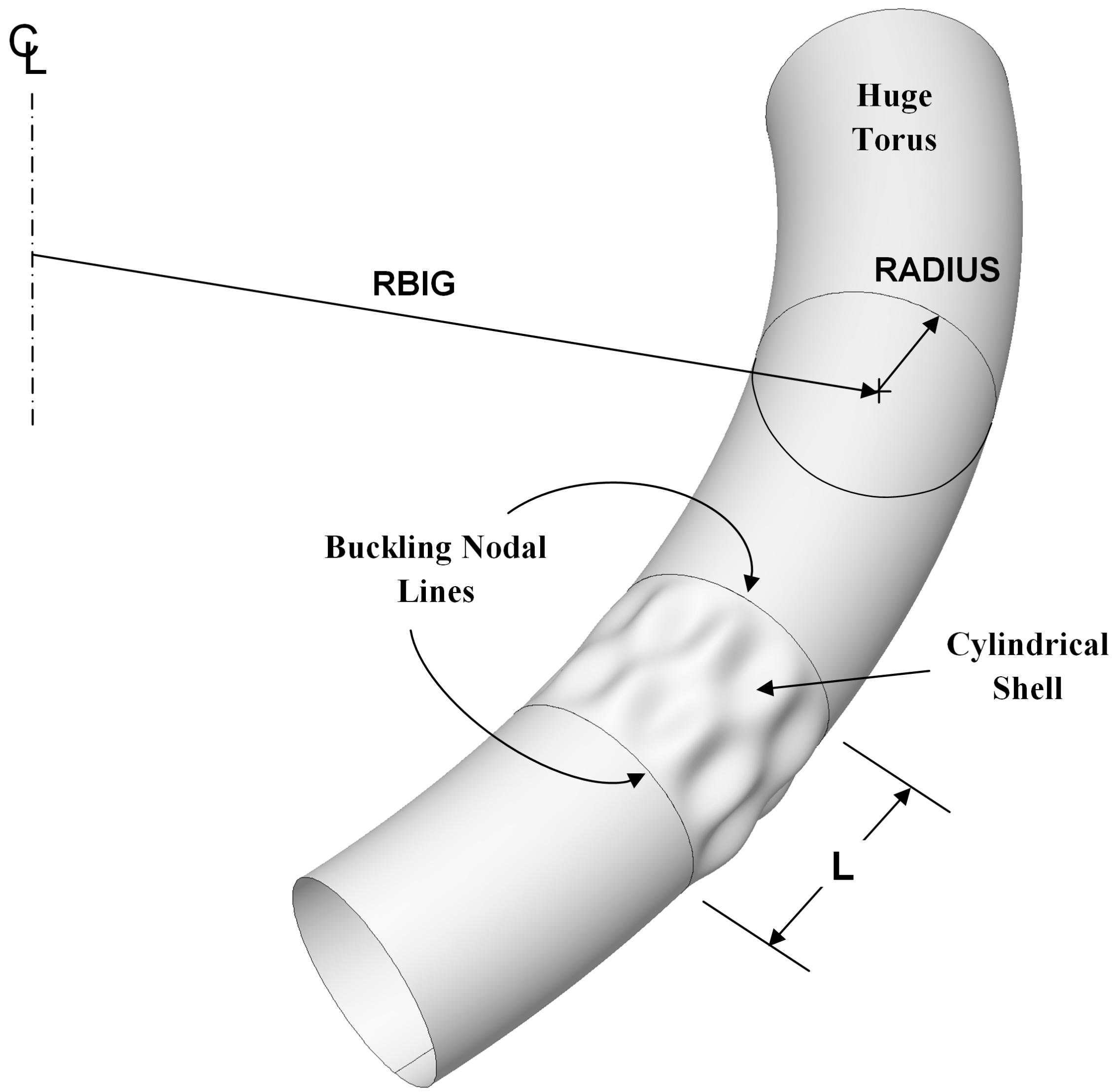

Fig. 3 **Schematic of a "huge torus" model [7-9].** This figure was created by Robert P. Thornburgh [9]. For most "huge torus" models [7], a good choice of RBIG is RBIG = 100xL/π. The double-walled cylindrical balloons studied here have RADIUS = 120 inches to the inner wall of the double-walled vacuum chamber. For the "true prismatic" shell model the kinematic relationships introduced recently into BIGBOSOR4 [8] correspond essentially to RBIG = infinity. In the "huge torus" [7] and "true prismatic shell" [8] models what is the axial coordinate in the usual model of a cylindrical shell becomes the circumferential coordinate in the "huge torus" model, and what is the circumferential coordinate in the usual model of a cylindrical shell becomes the meridional coordinate in the "huge torus" model. This "trick" of exchanging coordinates makes it possible to analyze prismatic shells as if they were shells of revolution. Hence, the details of the cross section of the double-wall of the balloon are retained, and a shell-of-revolution code such as BIGBOSOR4 can be used to analyze the cylindrical vacuum chamber that is not, in the ordinary sense, a shell of revolution. The wall characteristics need not be smeared, and both local and general buckling modes can be obtained.

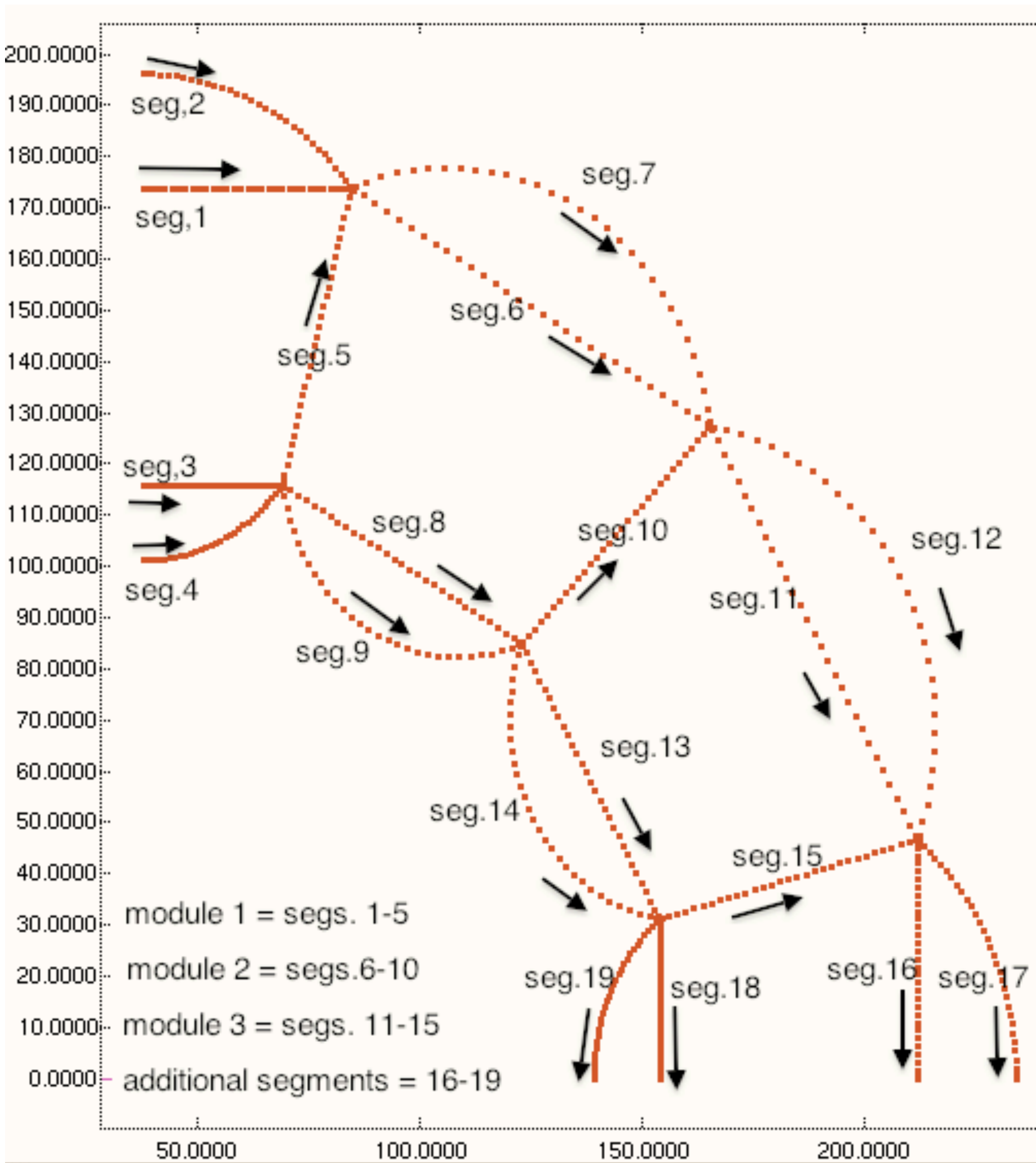

Fig. 4 The complex wall of the cylindrical vacuum chamber (balloon) consists of a number of modules, NMODUL. NMODUL is an input quantity that the end user chooses when executing the GENOPT processor, BEGIN. In this crude model of a balloon wall **with radial webs** NMODUL = 3. The “shell” segment numbering convention and the direction of “travel” along each segment in the BIGBOSOR4 model are displayed here. Each “shell” segment is discretized in the meridional coordinate: 31 nodal points per segment. Variation of the buckling modal displacements in the direction normal to the plane of the paper is trigonometric. Although the computer program, BIGBOSOR4, was created to analyze shells with finite bending stiffness and the segments of the vacuum chamber treated in this paper act more like membranes than like shells, useful predictions are obtained.

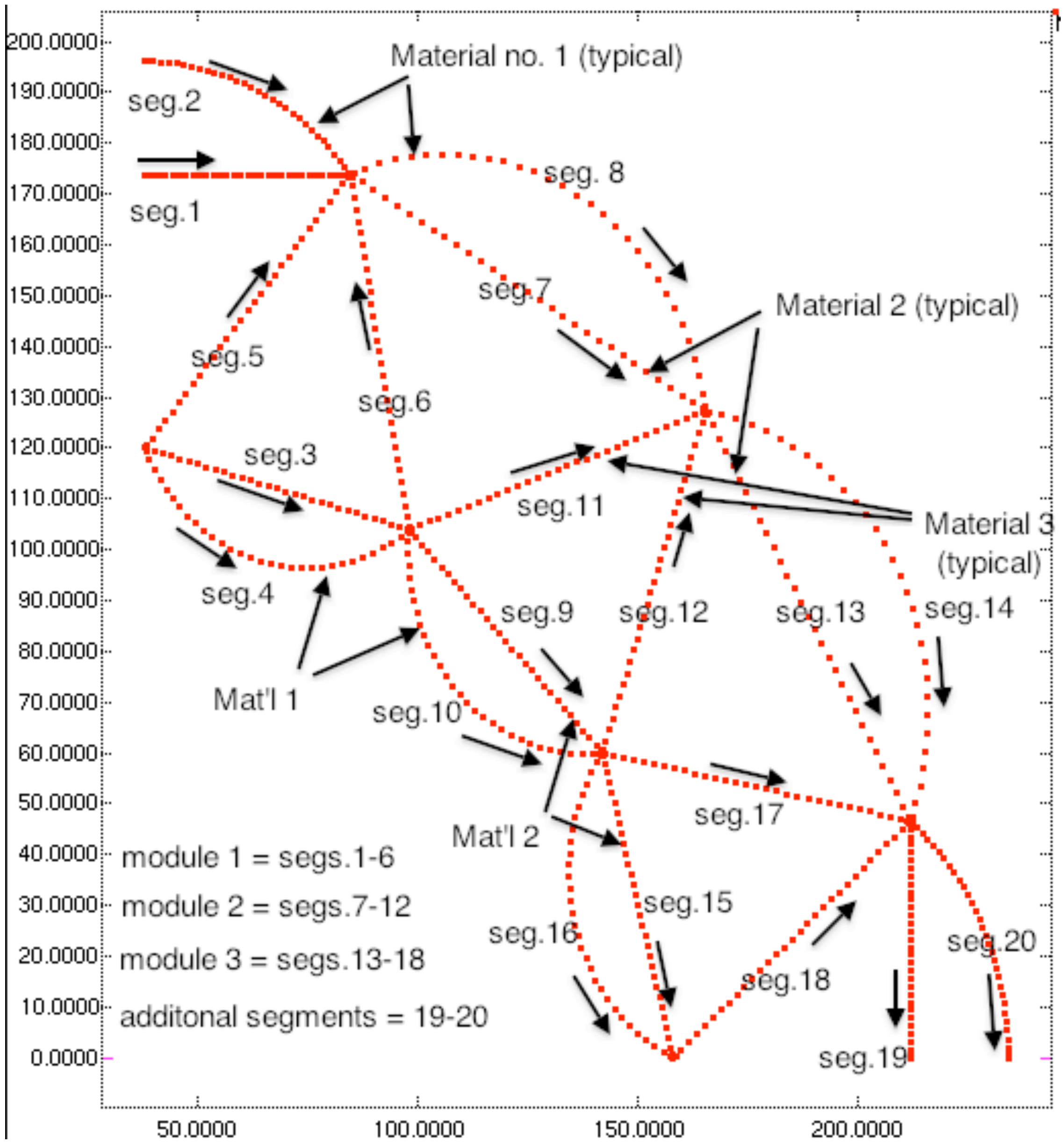

Fig. 5 The complex wall of the cylindrical vacuum chamber (balloon) consists of a number of modules, NMODUL. NMODUL is an input quantity that the end user chooses when executing the GENOPT processor, BEGIN. In this crude model of a balloon wall **with truss-like (slanted) webs** NMODUL = 3. The “shell” segment numbering convention and the direction of “travel” along each segment in the BIGBOSOR4 model are displayed here. Each “shell” segment is discretized in the meridional coordinate: 31 nodal points per segment. Variation of the buckling modal displacements in the direction normal to the plane of the paper is trigonometric. There are 3 material types in this model and also in the model shown in the previous figure. In the studies reported in this paper all three material types have the same properties. Although the computer program, BIGBOSOR4, was created to analyze shells with finite bending stiffness and the segments of the vacuum chamber treated in this paper act more like membranes than like shells, useful predictions are obtained.

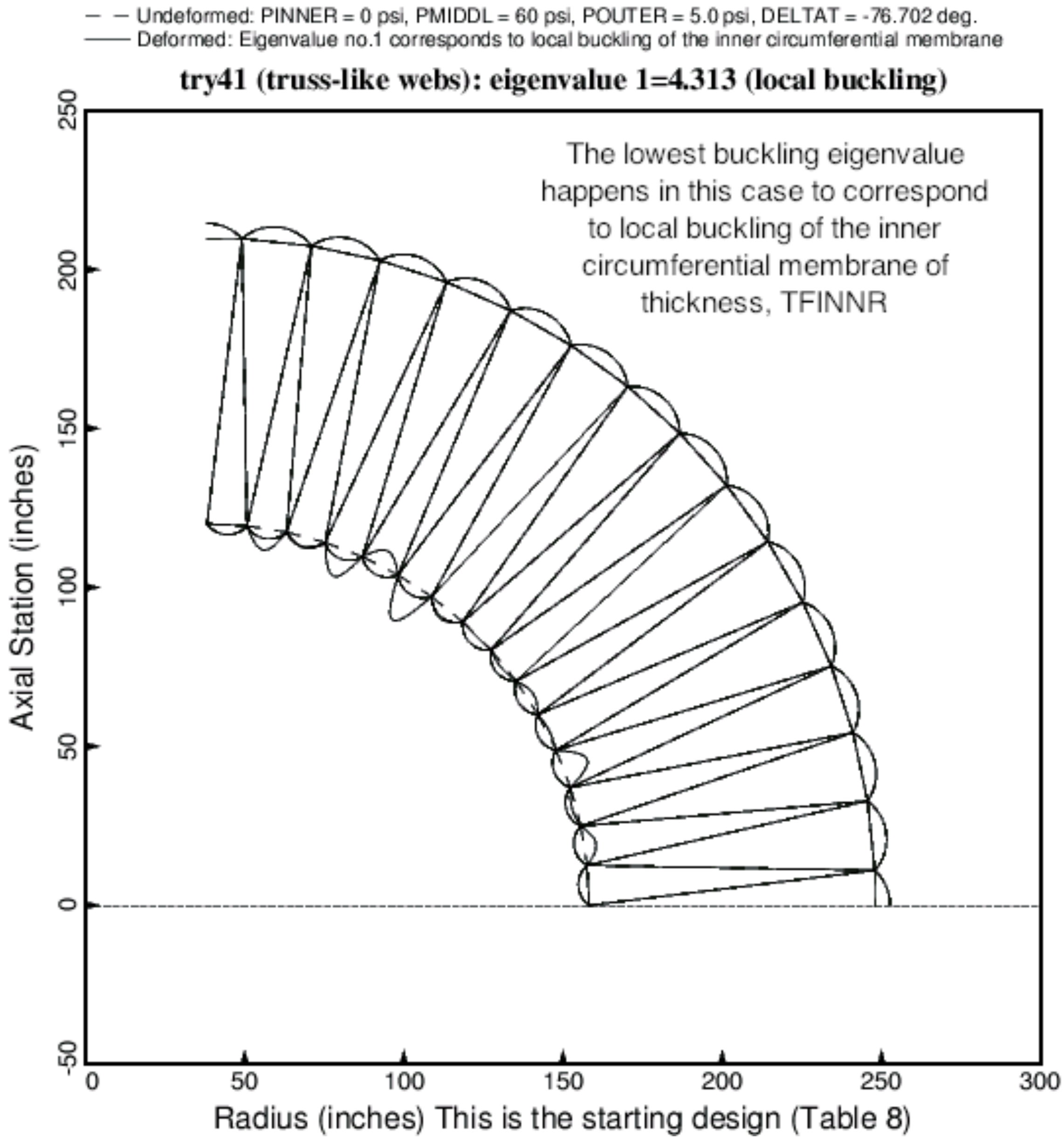

Fig. 6a The critical buckling mode of the starting design of the vacuum chamber with **truss-like (slanted) webs** and with NMODUL = 15 (15 modules). In every case explored in this paper the lowest **local** buckling eigenvalue (buckling load factor) corresponds to buckling (wrinkling) of the inner circumferential membrane with thickness, TFINNR. Sometimes, especially for the balloons with radial webs, the critical buckling mode (buckling mode associated with the lowest eigenvalue) corresponds to overall ovalization of the entire cross section of the balloon. See Fig. 23 for example. In all cases there are many, many local buckling eigenvalues clustered very closely. This clustering makes it difficult to find the eigenvalue associated with general buckling, unless that eigenvalue happens to be lower than the lowest local buckling eigenvalue. The starting design listed in Table 8 has HEIGHT = 90 inches, RINNER = 8 inches, ROUTER = 15 inches, and all five thicknesses, TINNER, TOUTER, TFINNR, TFOUTR, TFWEBS = 0.1 inch.

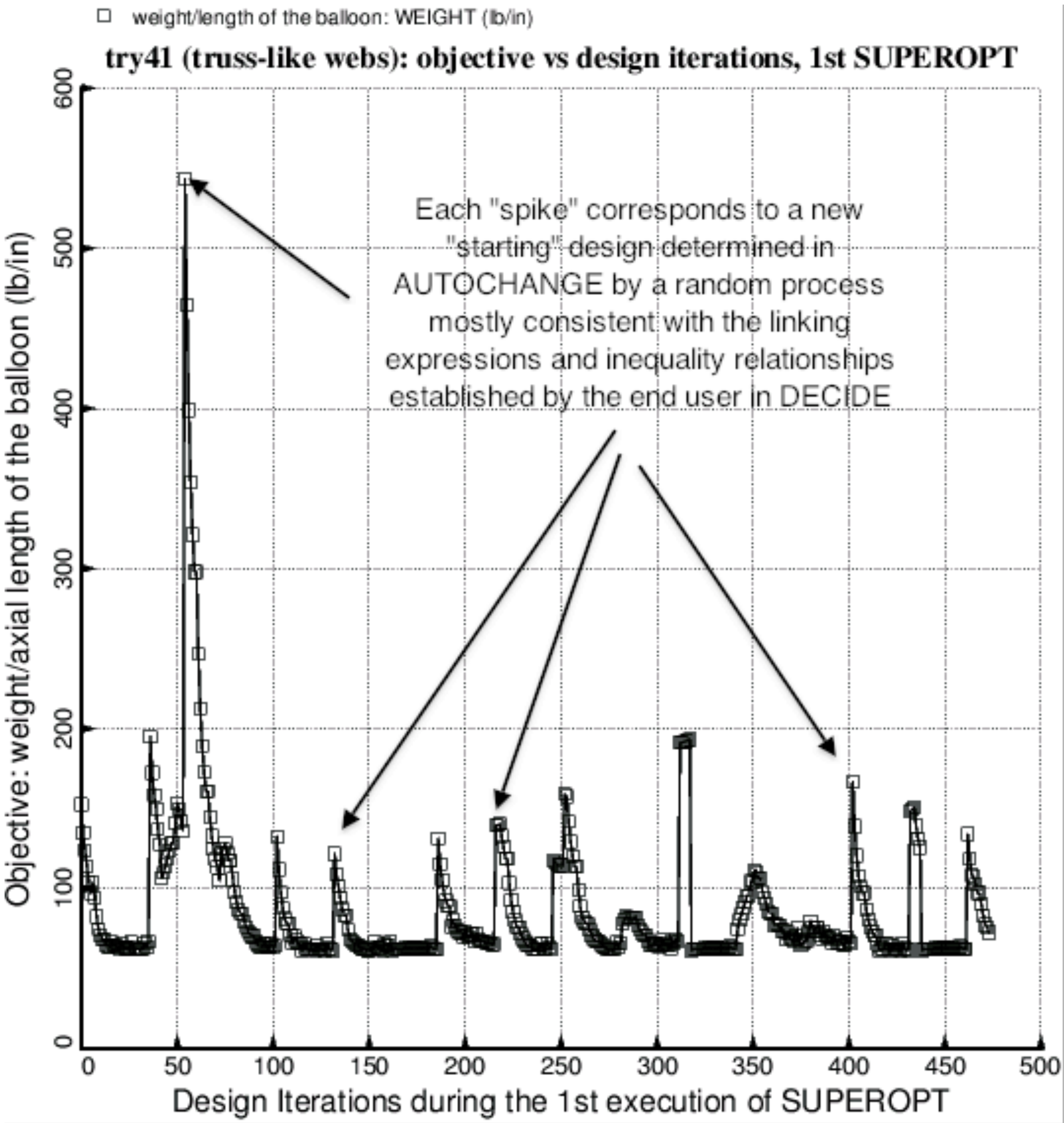

Fig. 6b Evolution of the objective (weight/axial length) during the first execution of the GENOPT processor called SUPEROPT. A successful and complete execution of SUPEROPT requires about 20 hours of computer time on the writer's workstation for the balloon with 15 modules over 90 degrees of circumference (previous figure). In this first execution of SUPEROPT the two radii, RINNER and ROUTER (Fig. 1) are not decision variables (Table 9). The optimum design obtained after the first execution of SUPEROPT is listed in Table 11 and archived with the use of the GENOPT processor called CHANGE (Table 12).

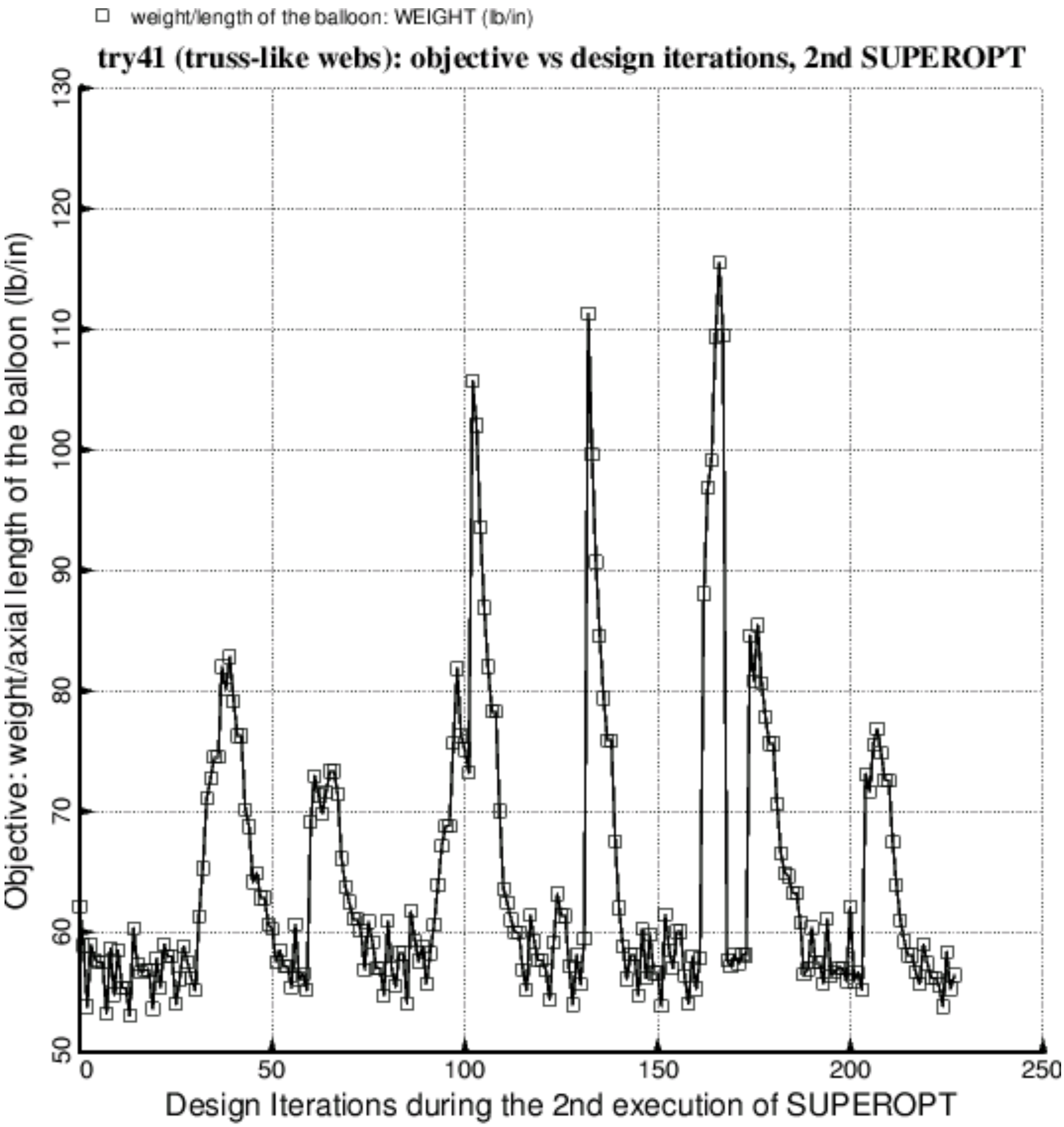

Fig. 7 Evolution of the objective (weight/axial length) during the second execution of the GENOPT processor, SUPEROPT. This 2nd execution of SUPEROPT was terminated on purpose because the writer did not want to wait for several hours for completion of the approximately 470 iterations specified by the GENOPT software. In this 2nd execution of SUPEROPT the two radii, RINNER and ROUTER (Fig. 1) are now decision variables (Table 13). The optimum design obtained after the second execution of SUPEROPT is listed in Table 14 and archived with the use of the GENOPT processor called CHANGE (Table 15).

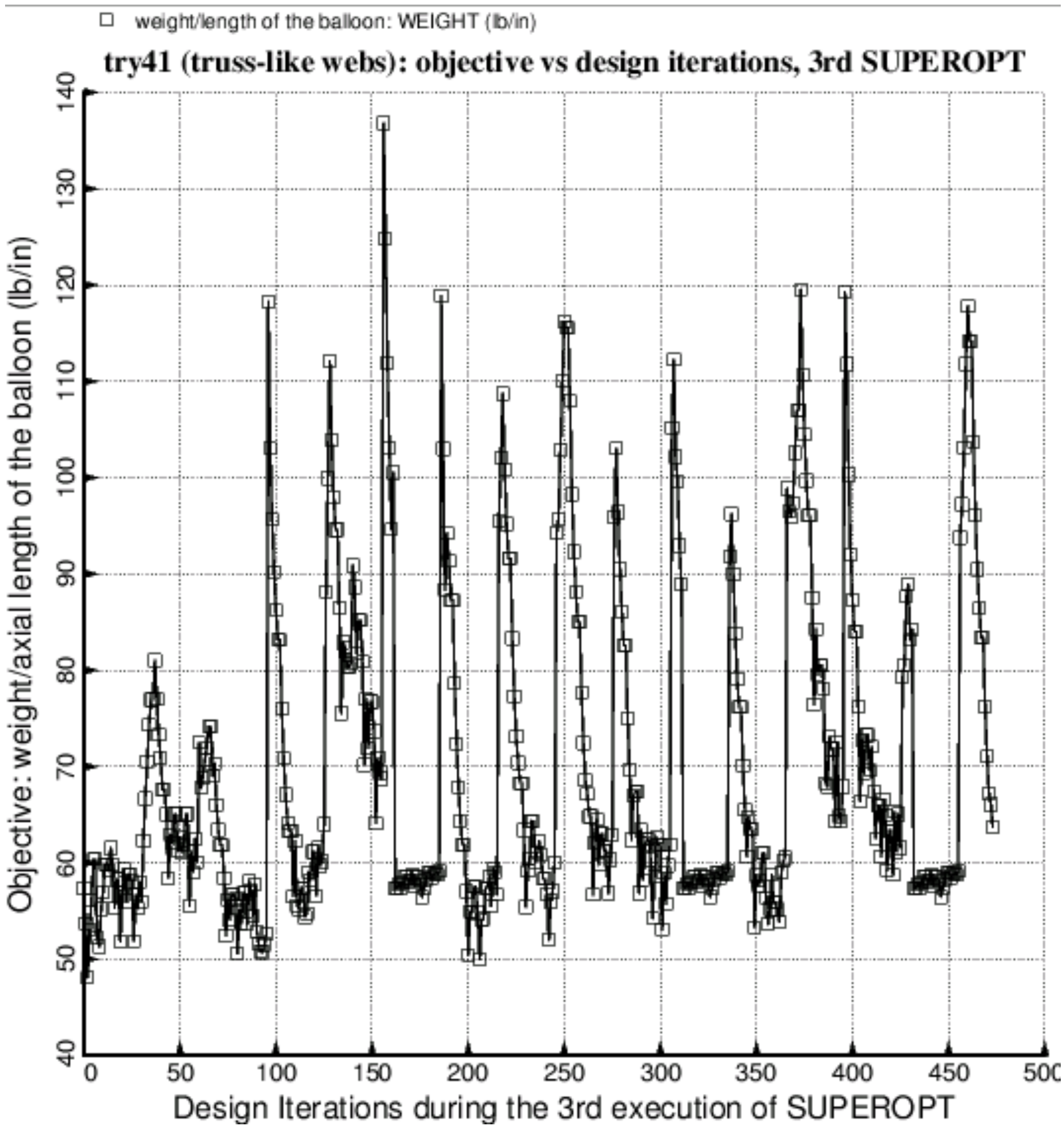

Fig. 8 Evolution of the objective (weight/axial length) during the third execution of the GENOPT processor, SUPEROPT. New lower bounds of the decision variables are specified in the execution of the GENOPT processor called DECIDE before the launch of this third execution of SUPEROPT (Table 16). The optimum design obtained after this third execution of SUPEROPT happens to be the same as that obtained after the second execution of SUPEROPT (Tables 14 and 15). Notice that starting at Design Iterations 155, 305, and 430 there is temporarily less jumpiness of the objective in successive design iterations. This happens because SUPEROPT temporarily resets the move limit of decision variables to a much more restrictive value in order to “close in” on a possibly better optimum design in the immediate neighborhood of whatever optimum has been determined up to that point in the long SUPEROPT process. In this particular case the exploration in the immediate neighborhood in design space did not result in a better optimum design.

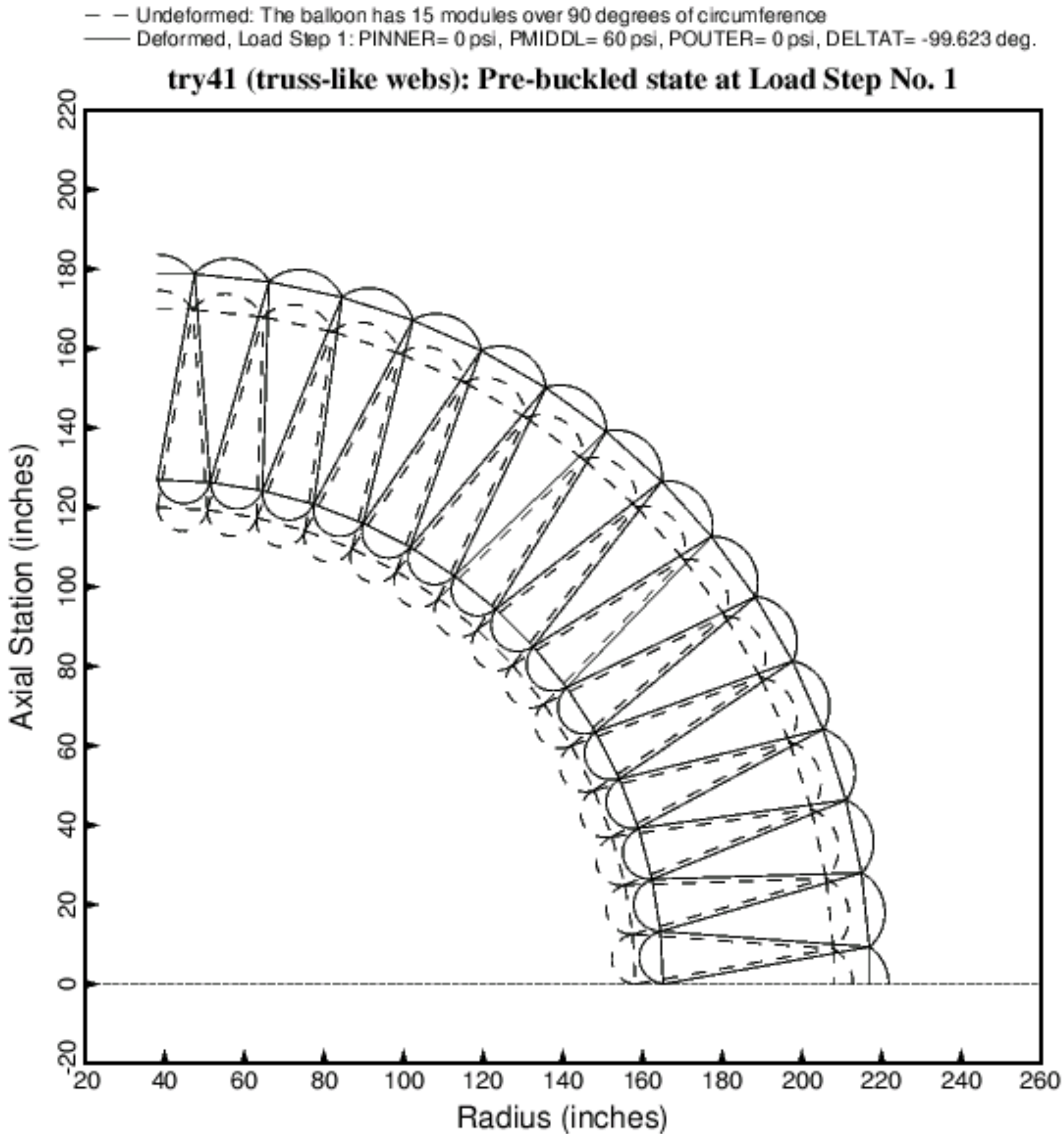

Fig. 9 Uniform pre-buckled state of the balloon with truss-like (slanted) webs subjected to the loads in Load Step No. 1, that is, before the outer pressure, POUTER = 15 psi, has been applied. As described in the text the delta-temperature, DELTAT = -99.623, is applied in order to generate the correct pre-buckling axial tension produced by PINNER because the ends of the cavity between the inner and outer walls is assumed to be sealed at the two ends of the cylindrical vacuum chamber. Note: plots of this type, generated via a BIGBOSOR4 input file called “try4.BEHX2”, can no longer be obtained without modifying SUBROUTINE BEHX2 as described in **Item 8** of **Section 8**.

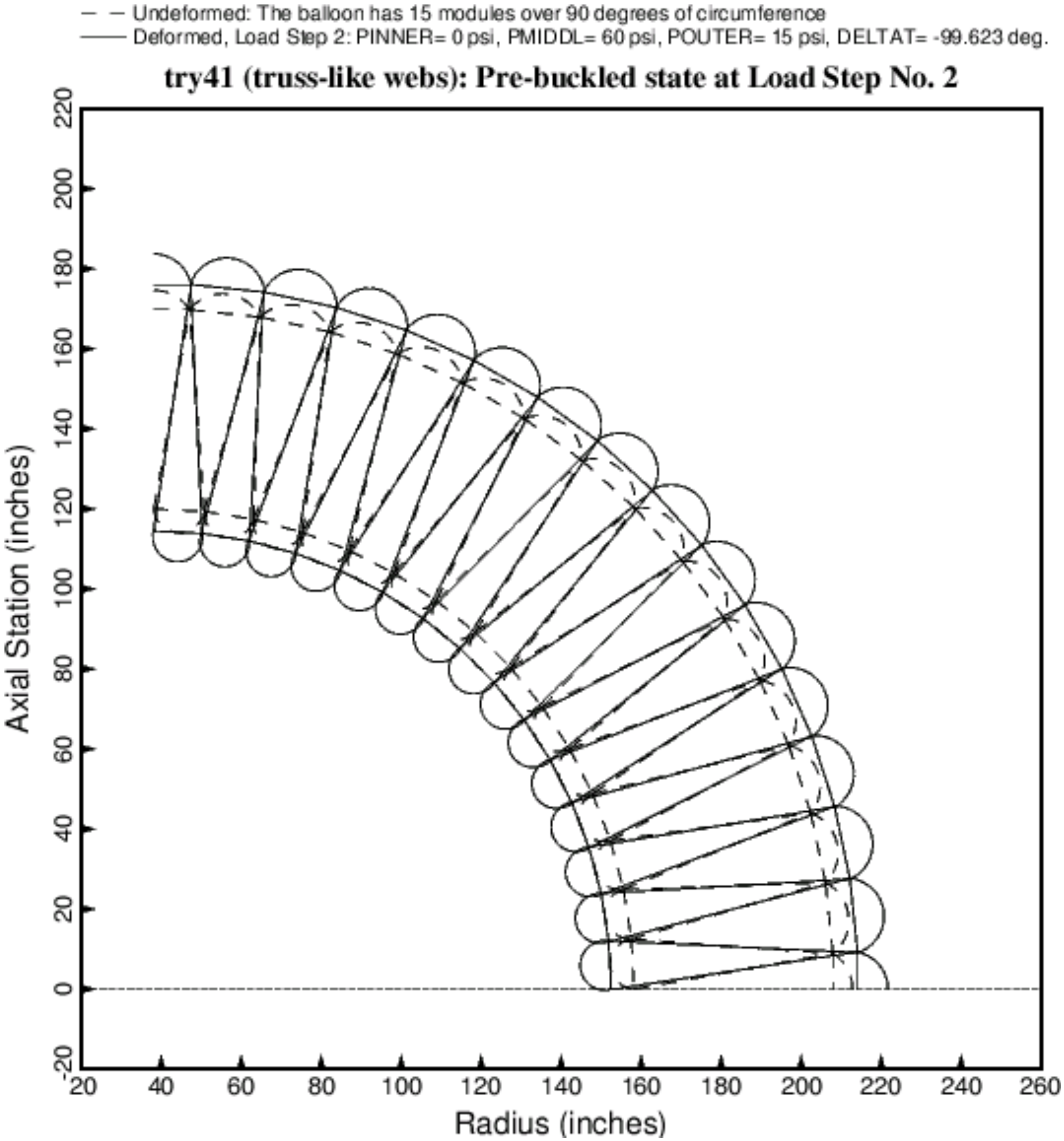

Fig. 10 Uniform pre-buckled state of the balloon subjected to the loads in Load Step No. 2, that is, after the outer pressure, POUTER, has been applied. In this example POUTER = 15 psi, and the wall cross section has been optimized. The results for POUTER = 15 psi and factor of safety for buckling of 1.0 are listed in Table 17. Note: plots of this type, generated via a BIGBOSOR4 input file called "try4.BEHX2", can no longer be obtained without modifying SUBROUTINE BEHX2 as described in **Item 8** of **Section 8**.

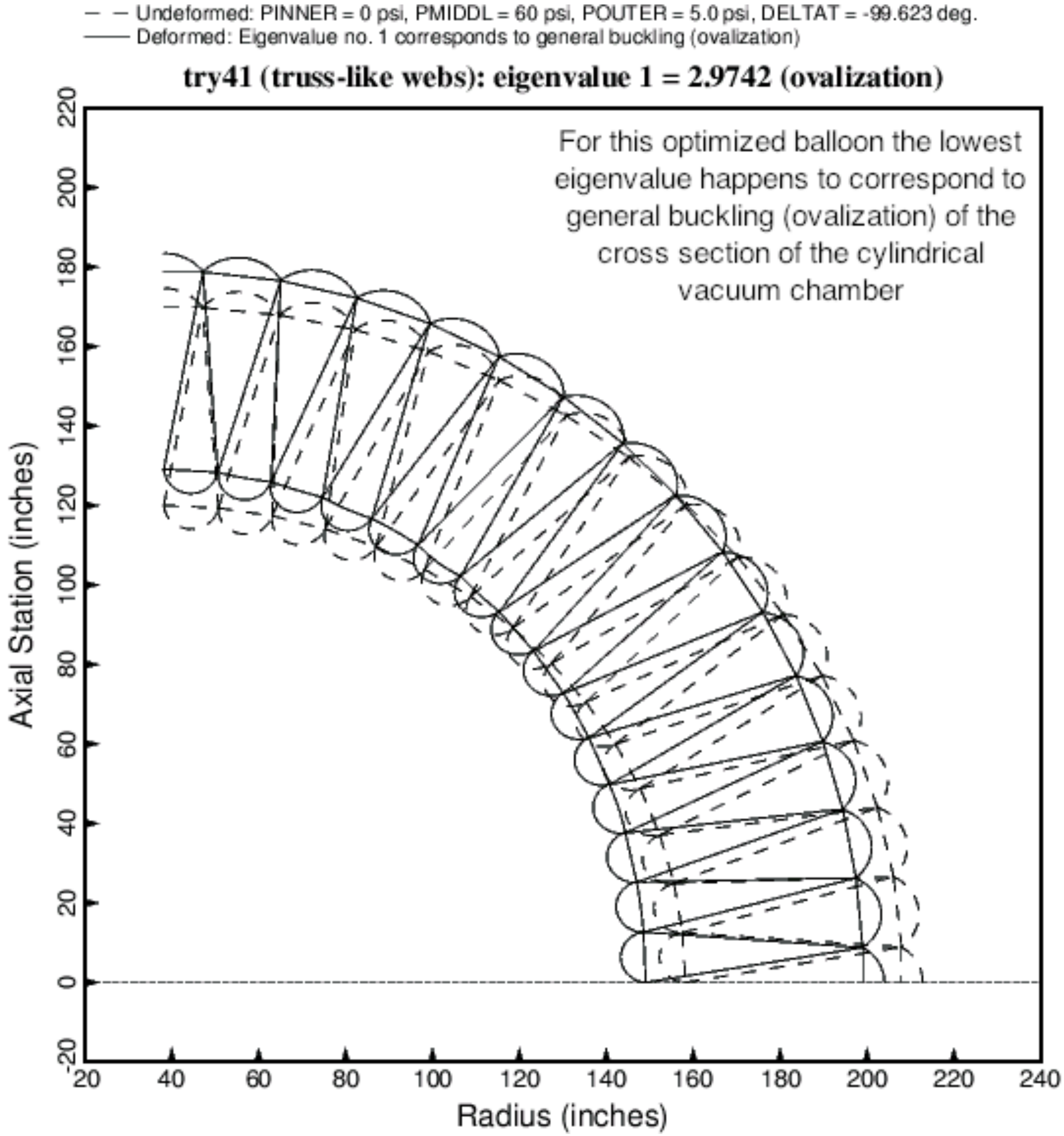

Fig. 11 The critical buckling mode and load factor (eigenvalue) corresponding to the optimized balloon cross section (Table 14). In this case the critical buckling mode, that is, the buckling mode associated with the lowest eigenvalue, happens to correspond to general buckling (ovalization) of the entire cross section of the cylindrical vacuum chamber. The buckling modes corresponding to some slightly higher eigenvalues are displayed in the next three figures.

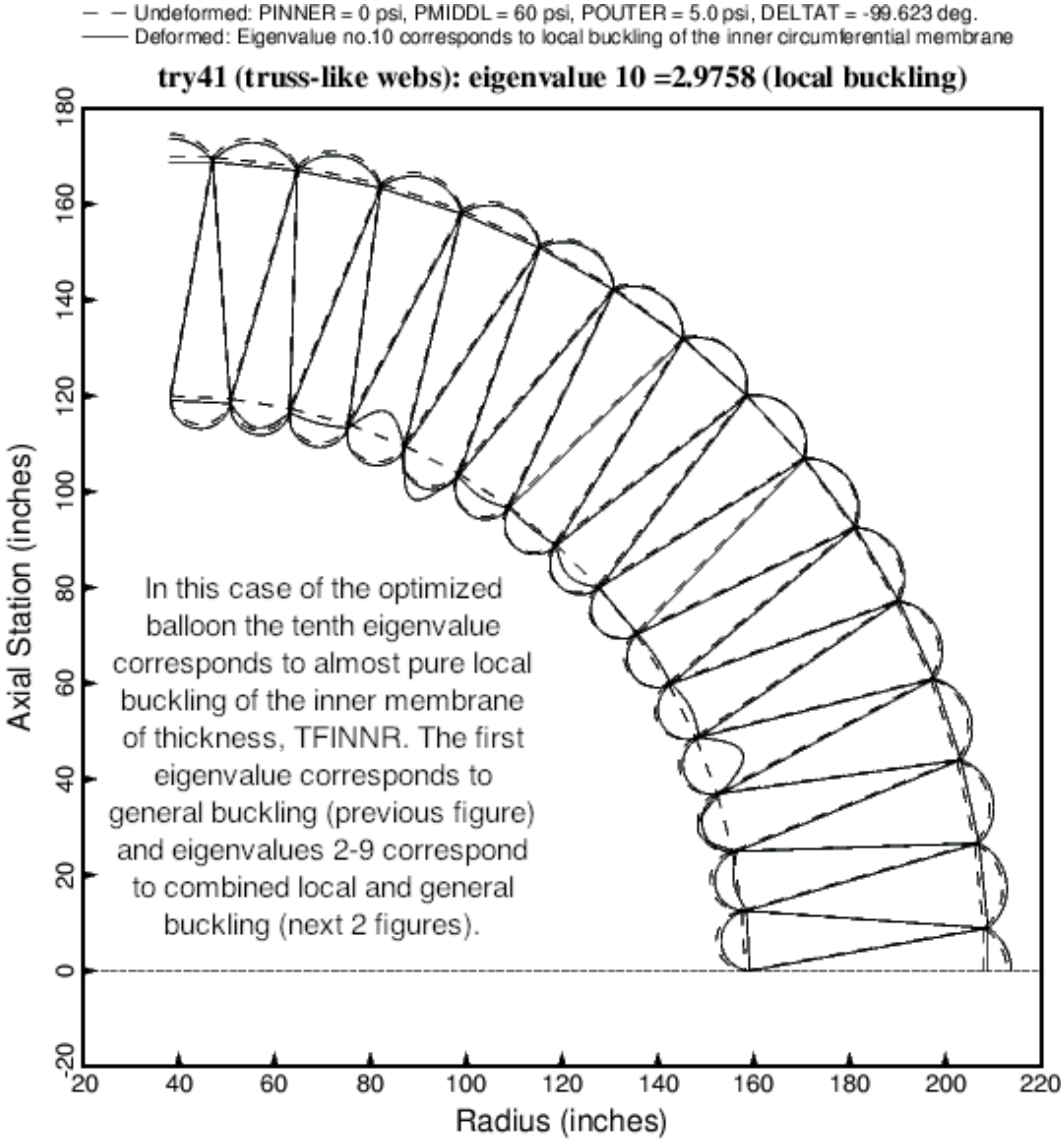

Fig. 12 The tenth buckling mode and load factor (eigenvalue) corresponding to the optimized balloon cross section (Table 14). The tenth buckling mode is the first mode that is almost entirely local buckling. There is a tiny component of general buckling (ovalization) contained in this tenth buckling mode. The buckling modes corresponding to the second and third eigenvalues are displayed in the next two figures.

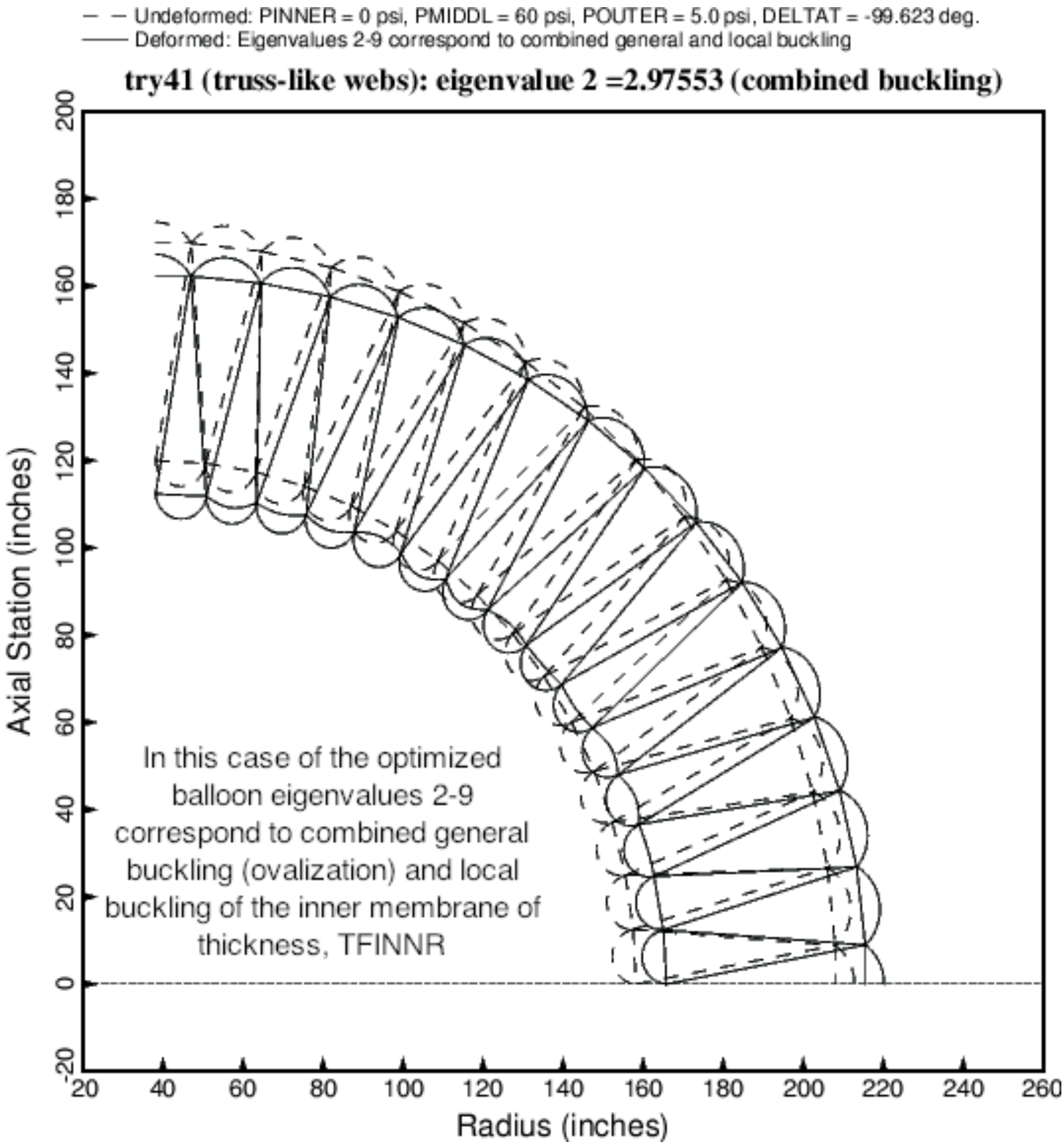

Fig. 13 The second buckling mode and load factor (eigenvalue) corresponding to the optimized balloon cross section (Table 14). The second buckling mode is a combination of local and general buckling.

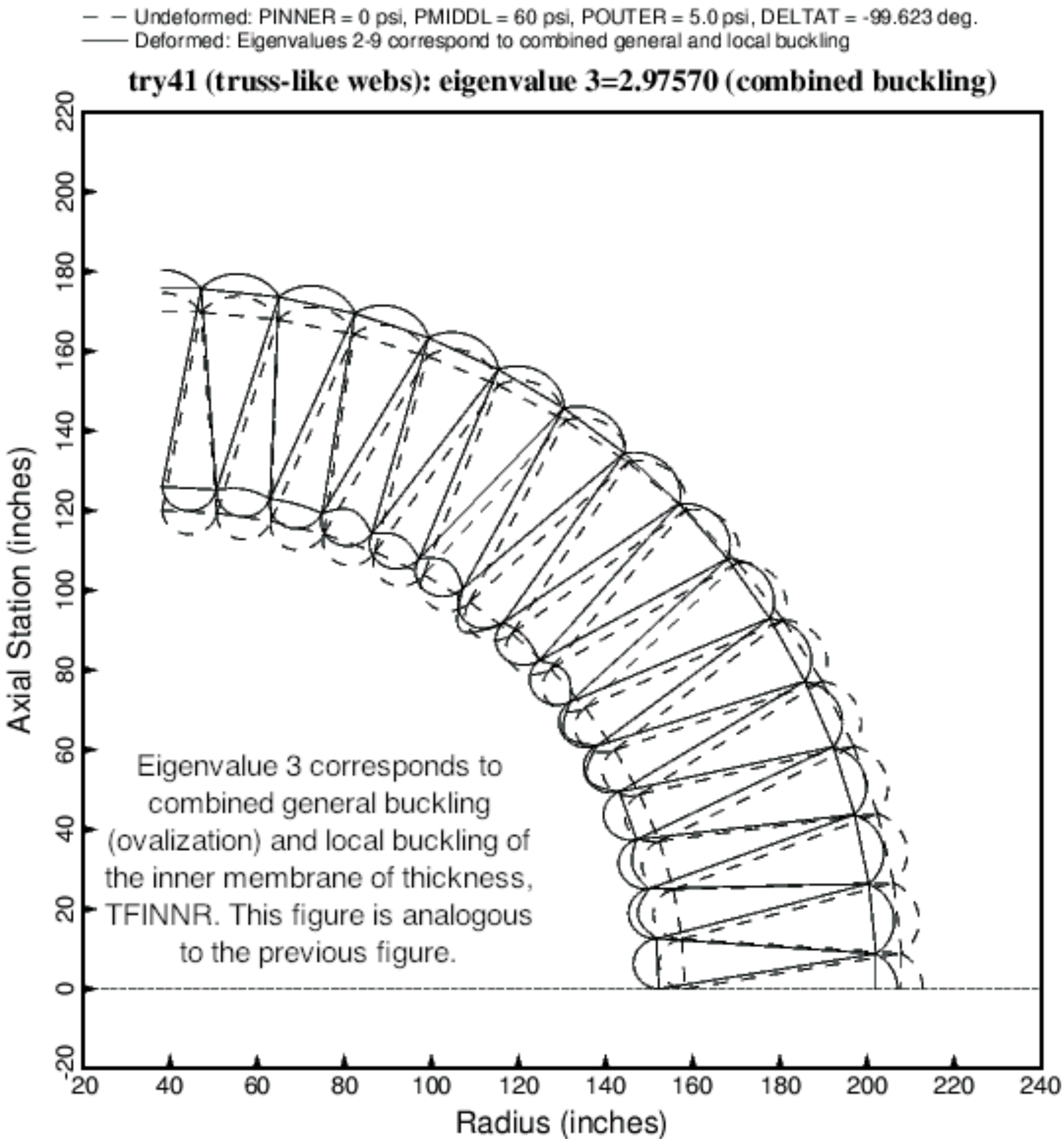

Fig. 14 The third buckling mode and load factor (eigenvalue) corresponding to the optimized balloon cross section (Table 14). The third buckling mode, like the second displayed in the previous figure, is a combination of local and general buckling.

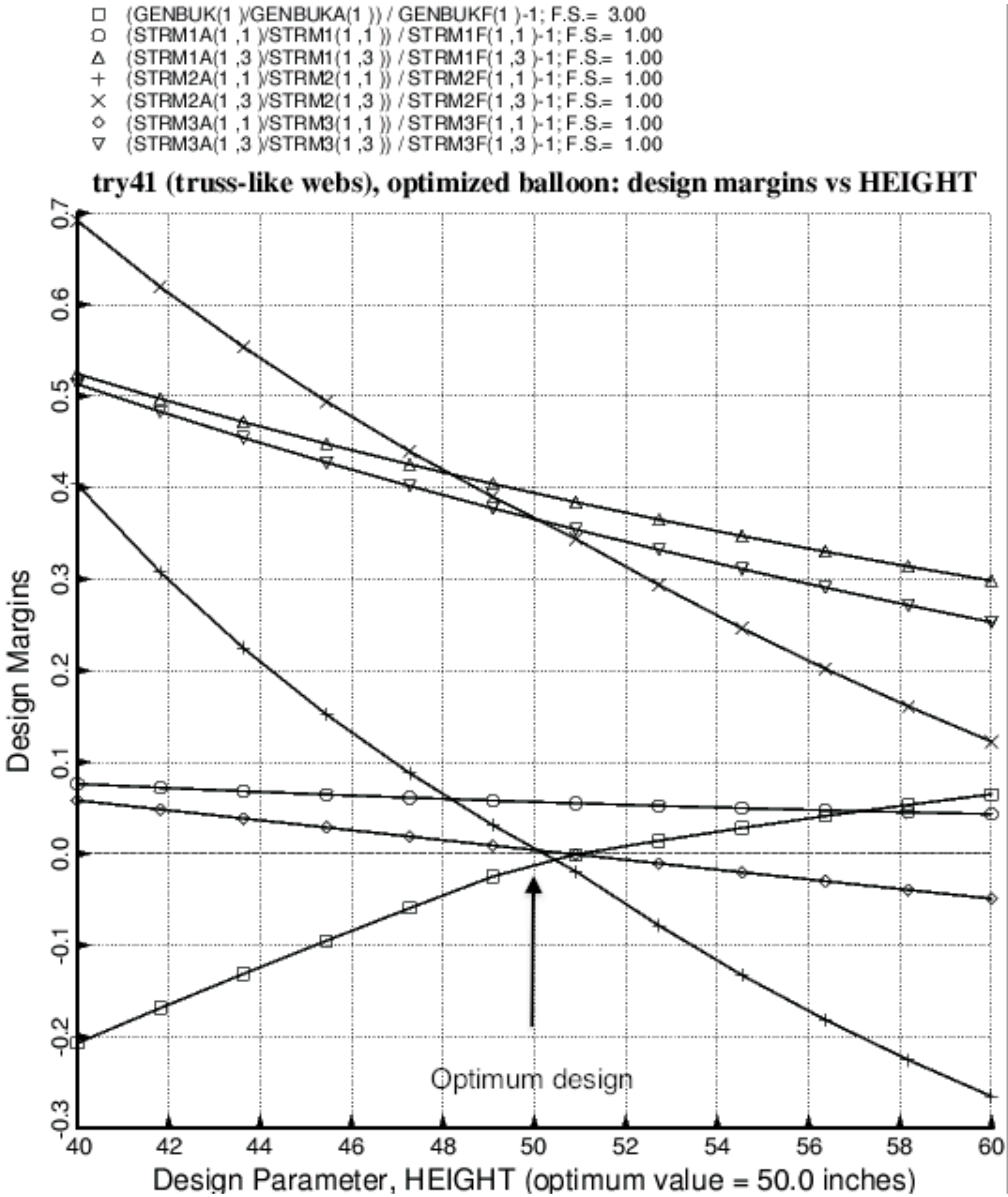

Fig. 15 Design sensitivity analysis of the optimized balloon (Table 14). This figure is produced following an analysis type, ITYPE = 3, in the *.OPT file (input for the GENOPT processor called MAINSETUP). In this case the design sensitivity with respect to the decision variable, HEIGHT, is determined. As is often the case for optimized designs, several design margins are critical (near zero) in the neighborhood of the optimum value of HEIGHT. (HEIGHT is the distance from the inner to outer walls of the balloon, as indicated in Fig. 1.)

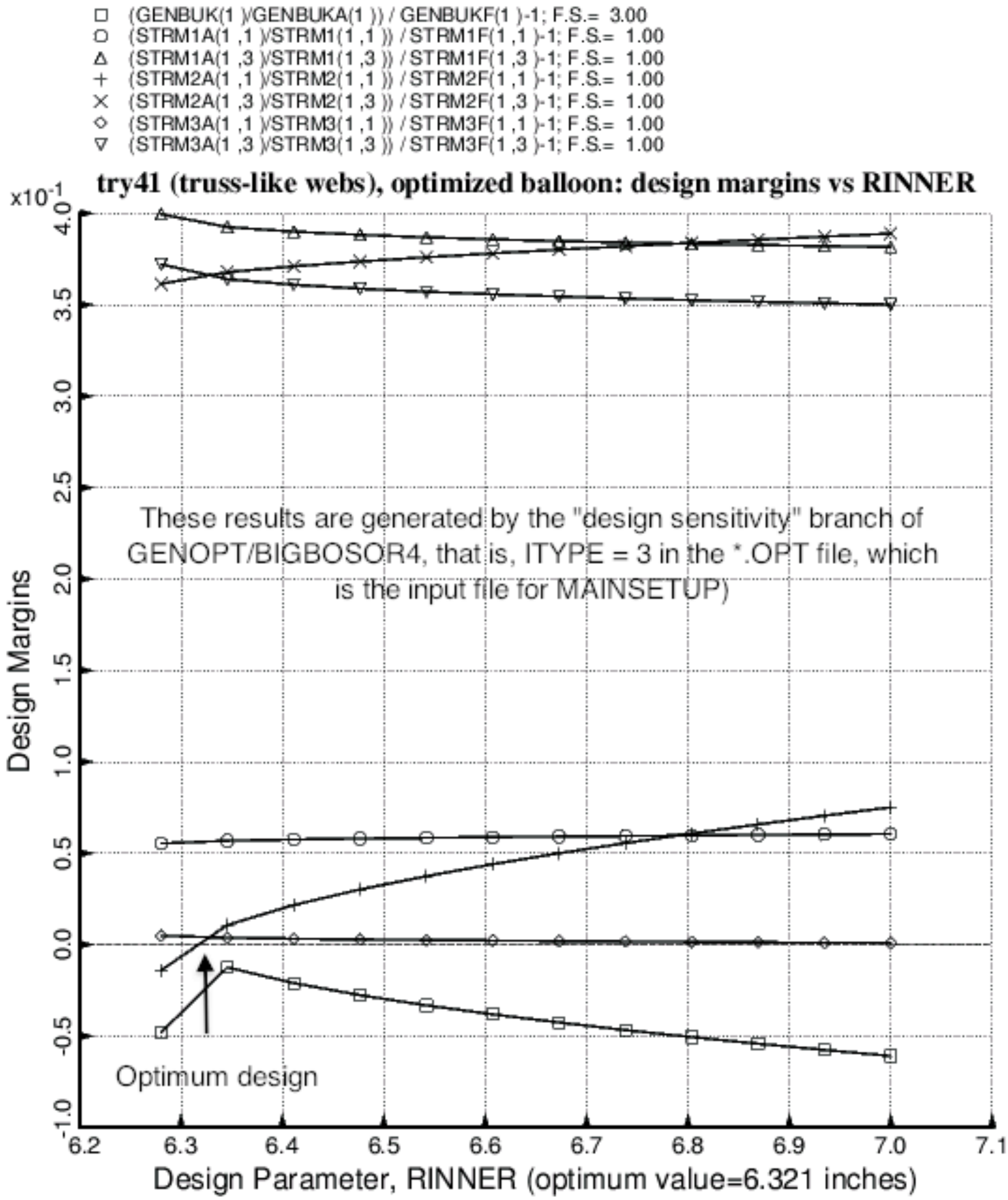

Fig. 16 Design sensitivity analysis of the optimized balloon (Table 14). This figure is produced following an analysis type, ITYPE = 3, in the *.OPT file (input for the GENOPT processor called MAINSETUP). In this case the design sensitivity with respect to the decision variable, RINNER, is determined. As is often the case for optimized designs, several design margins are critical (near zero) in the neighborhood of the optimum value of RINNER. (RINNER is the radius of curvature of the inner curved membrane in the balloon wall, as indicated in Fig. 1.)

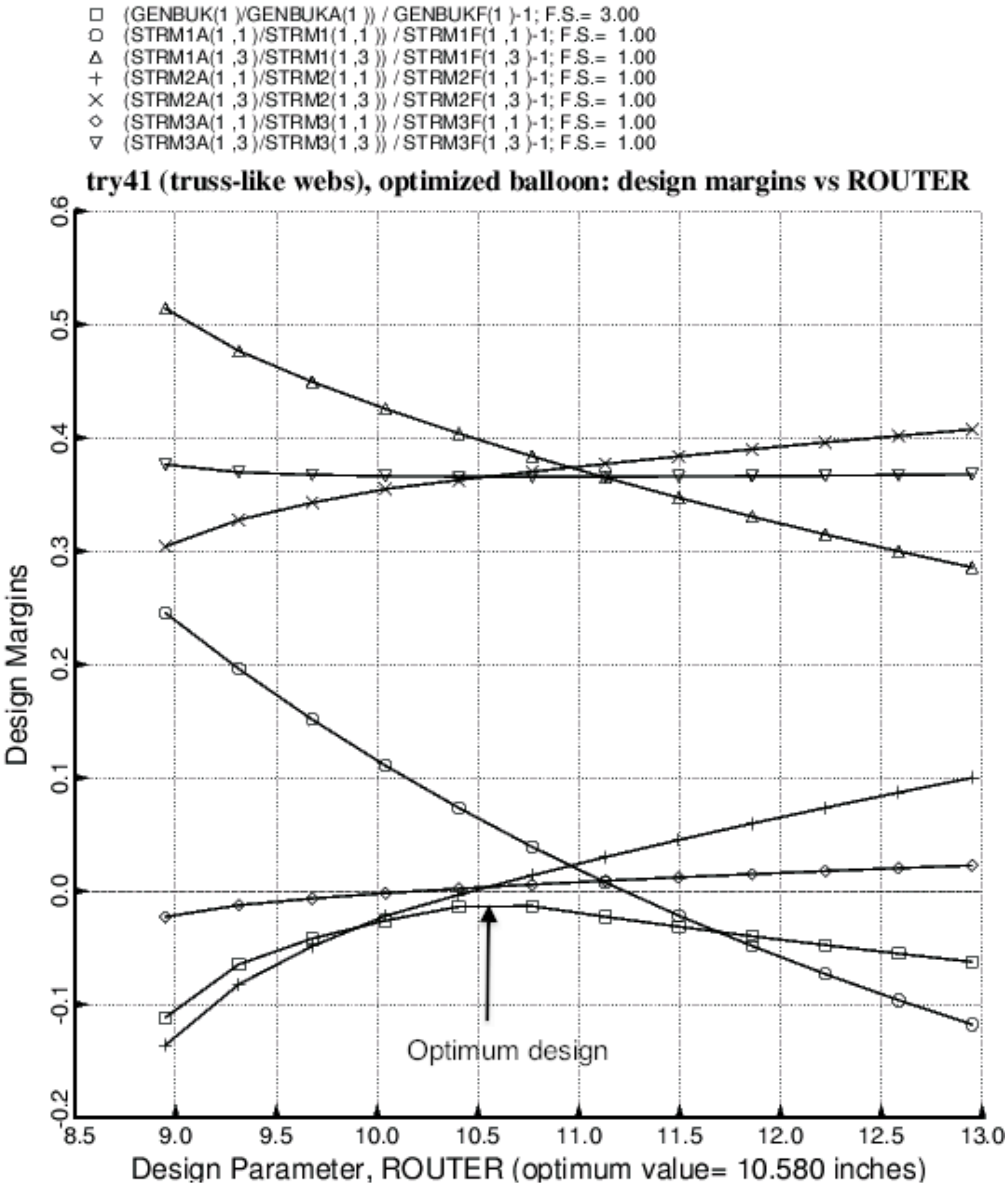

Fig. 17 Design sensitivity analysis of the optimized balloon (Table 14). This figure is produced following an analysis type, ITYPE = 3, in the *.OPT file (input for the GENOPT processor called MAINSETUP). In this case the design sensitivity with respect to the decision variable, ROUTER, is determined. As is often the case for optimized designs, several design margins are critical (near zero) in the neighborhood of the optimum value of ROUTER. (ROUTER is the radius of curvature of the outer curved membrane in the balloon wall, as indicated in Fig. 1.)

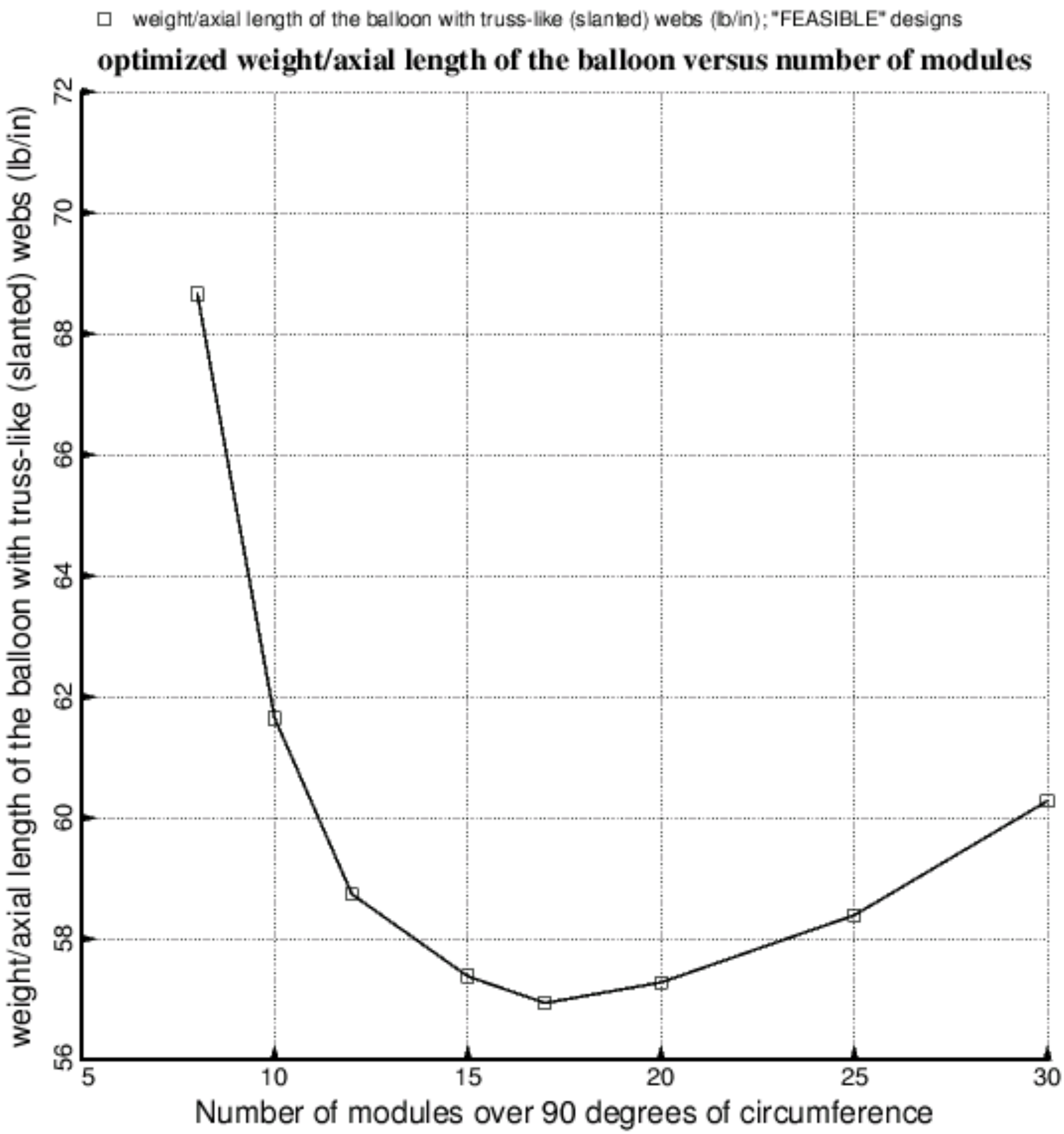

Fig. 18 Optimized weight/axial length as a function of the number, NMODUL, of modules in the model. These results required many days to obtain because the SUPEROPT runs required, especially for the models with 20 or more modules, long execution times on the computer.

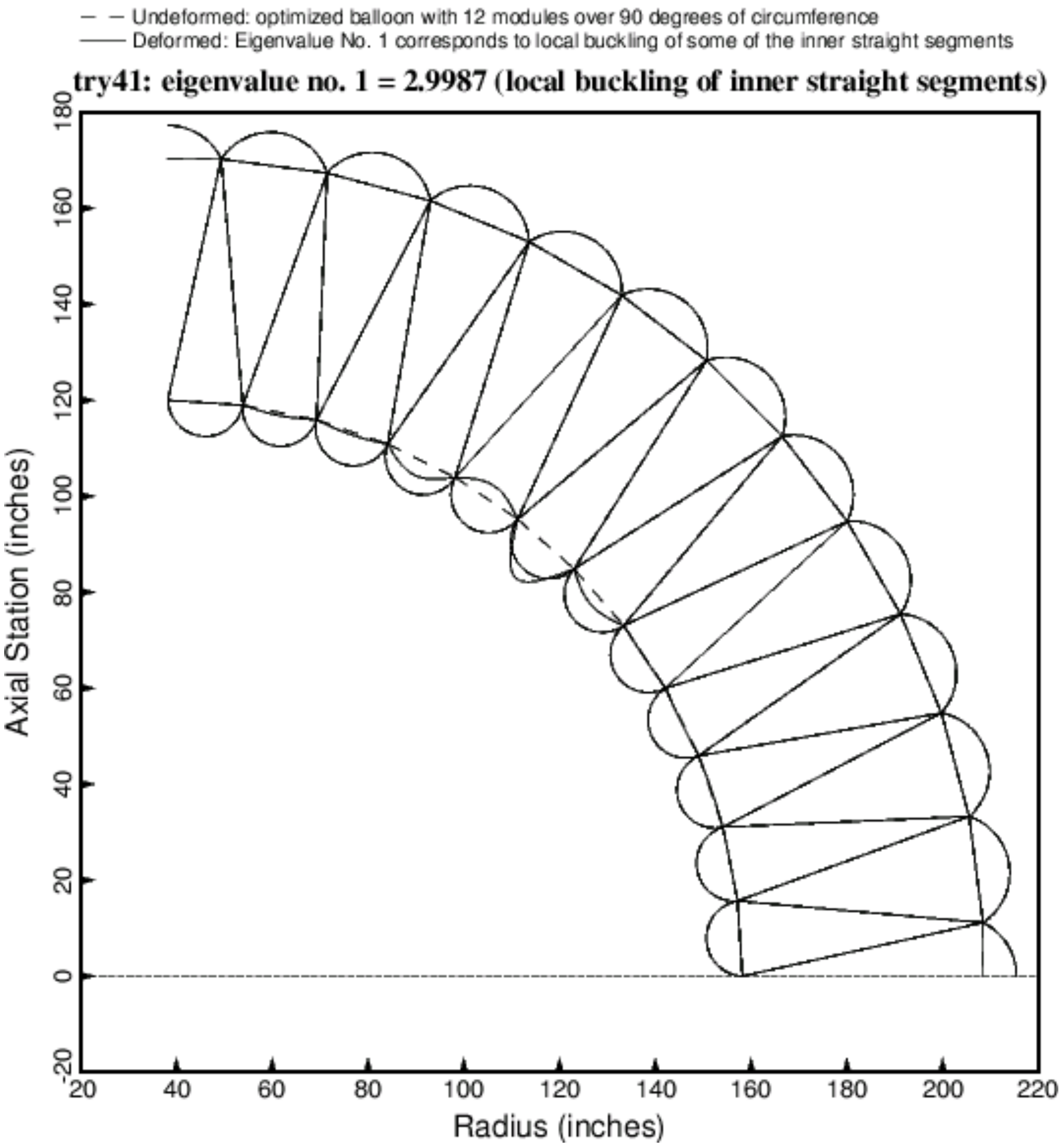

Fig. 19 Critical buckling mode of the optimized balloon with 12 modules over 90 degrees of circumference. In this particular case the critical (lowest) eigenvalue happens to be associated with a local buckling mode.

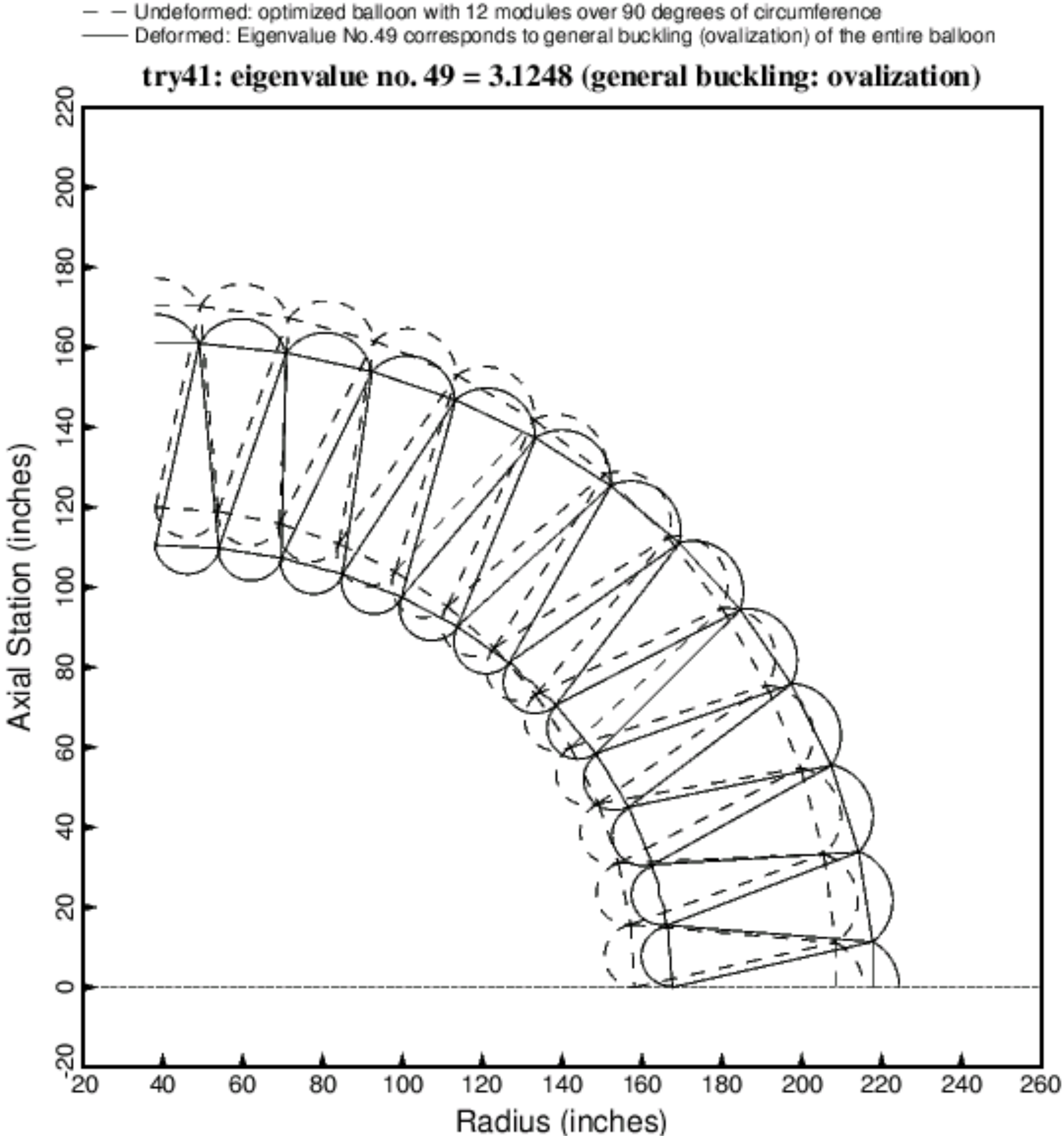

Fig. 20 49th buckling mode of the optimized balloon with 12 modules over 90 degrees of circumference. In this particular case the 49th eigenvalue happens to be associated with the general buckling (ovalization) mode.

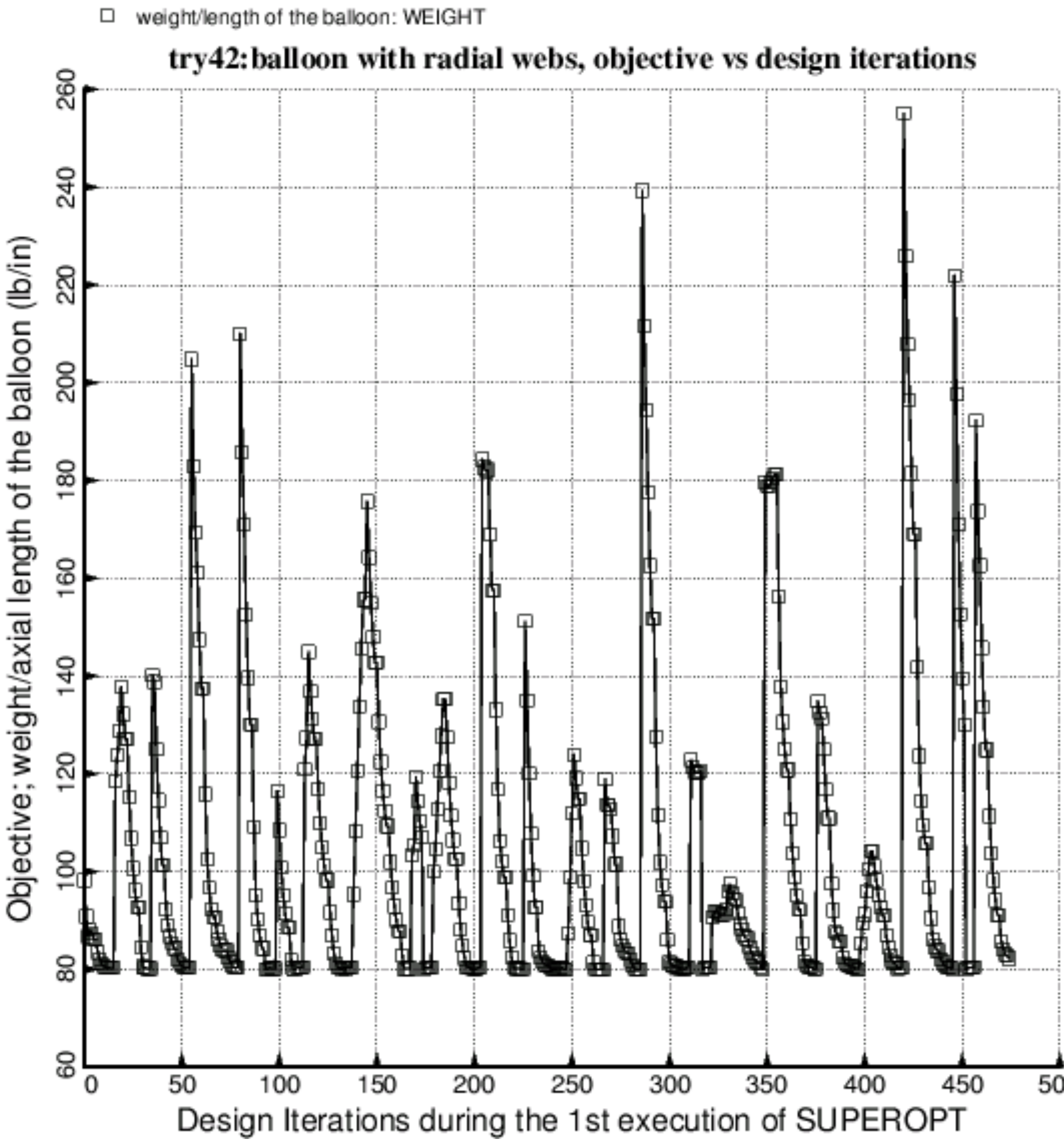

Fig. 21 This figure is analogous to Fig. 6b. Optimization of the balloon with **radial webs** (Fig.1). There are 15 modules over 90 degrees of circumference. In this first execution of SUPEROPT the radii, RINNER and ROUTER, are not decision variables.

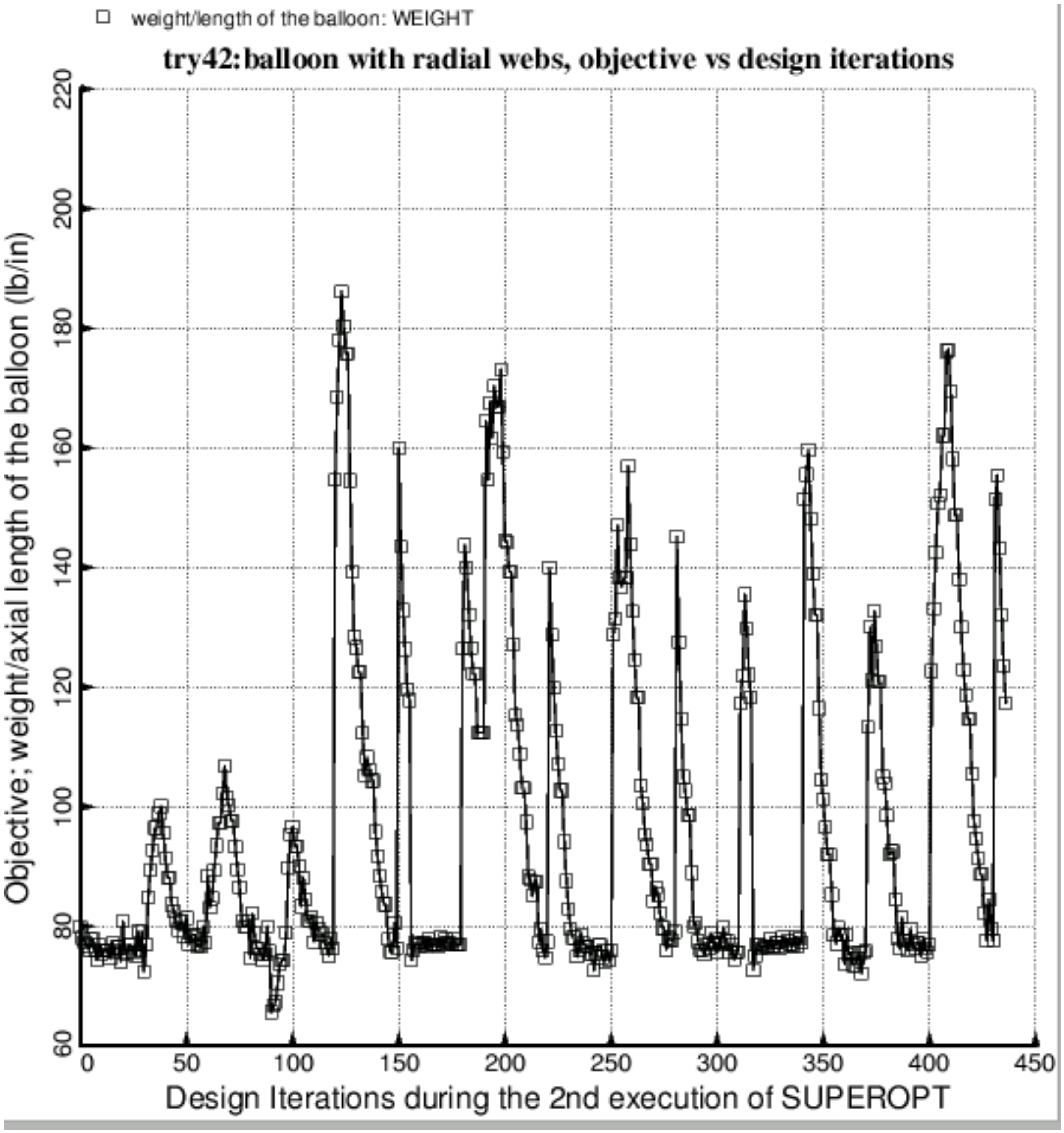

Fig. 22 This figure is analogous to Fig. 7. Optimization of the balloon with **radial webs** (Fig.1). In this second execution of SUPEROPT the radii, RINNER and ROUTER, are decision variables.

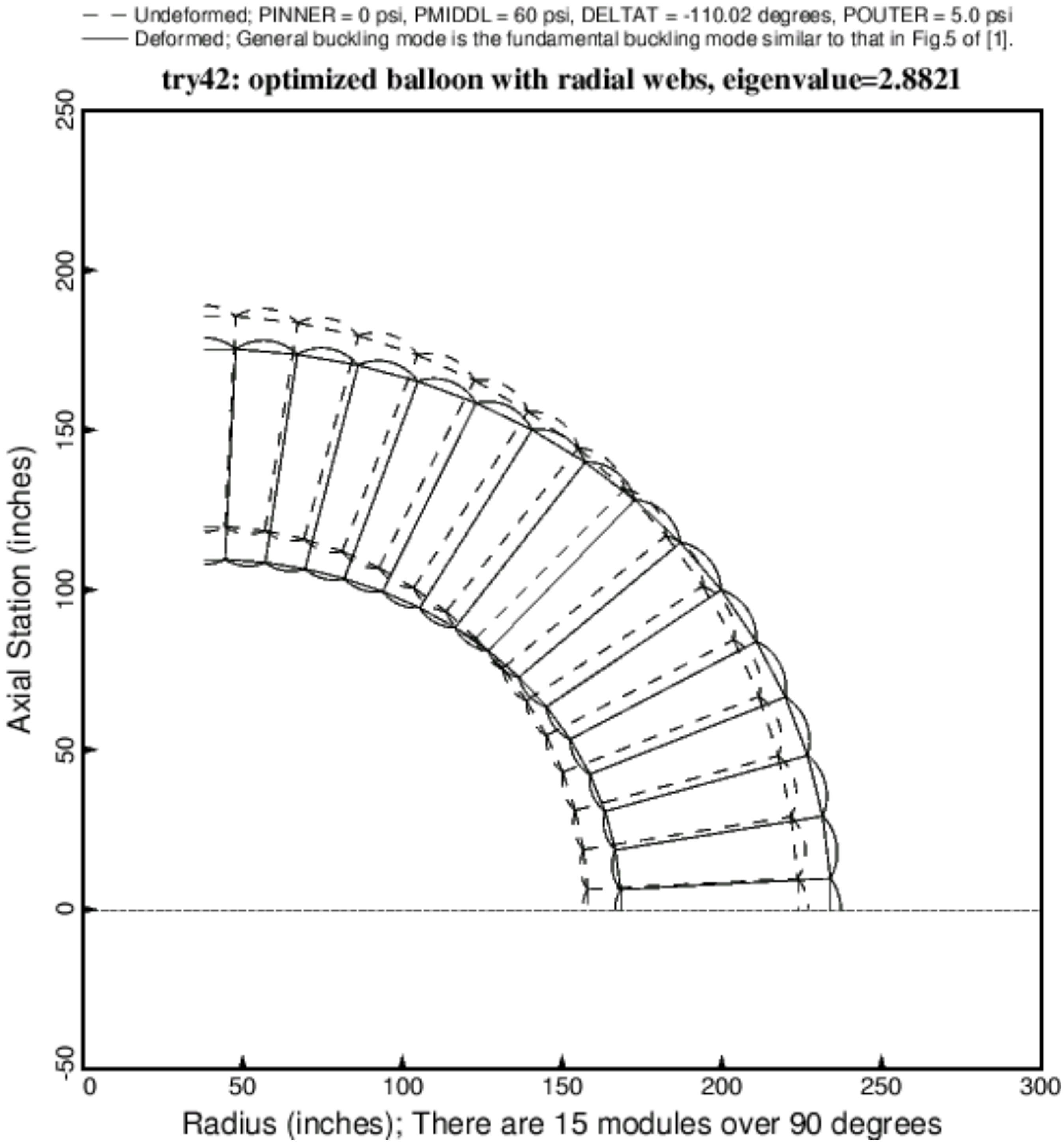

Fig. 23 This figure is analogous to Fig. 11. The critical buckling mode corresponds to general buckling (ovalization). This general buckling mode is similar to the general buckling mode shown in Fig. 5 of [1]. Notice, however, that there is less shearing deformation in the plane of the wall cross section at 45 degrees than exists in Fig. 5 of [1].

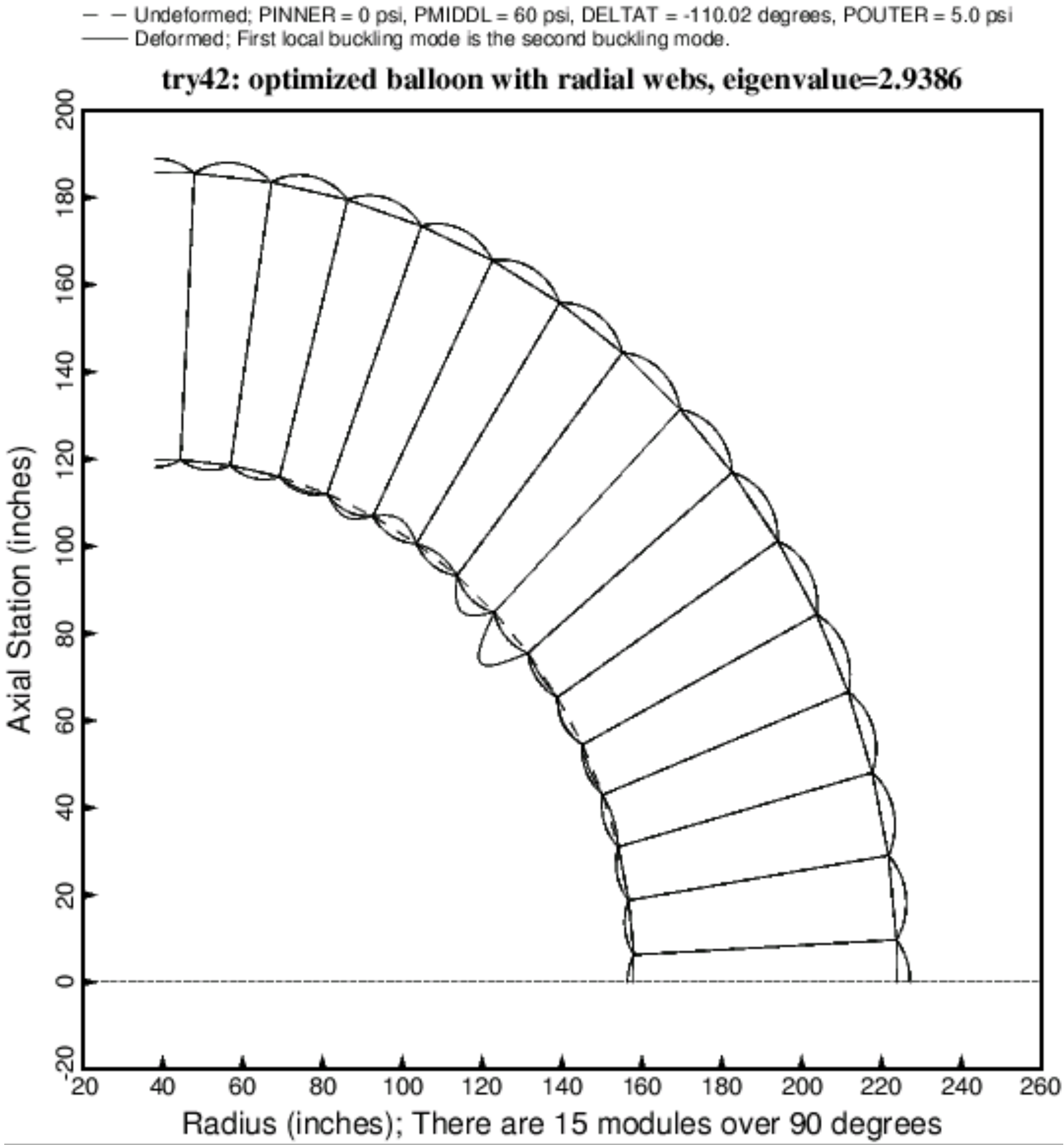

Fig. 24 This figure is analogous to Fig. 12. Local buckling of the optimized balloon with **radial webs**. At the optimum design the local buckling load factor, 2.9386, which corresponds to eigenvalue no. 2, is fairly close to the general buckling load factor, 2.8821, shown on the previous slide.

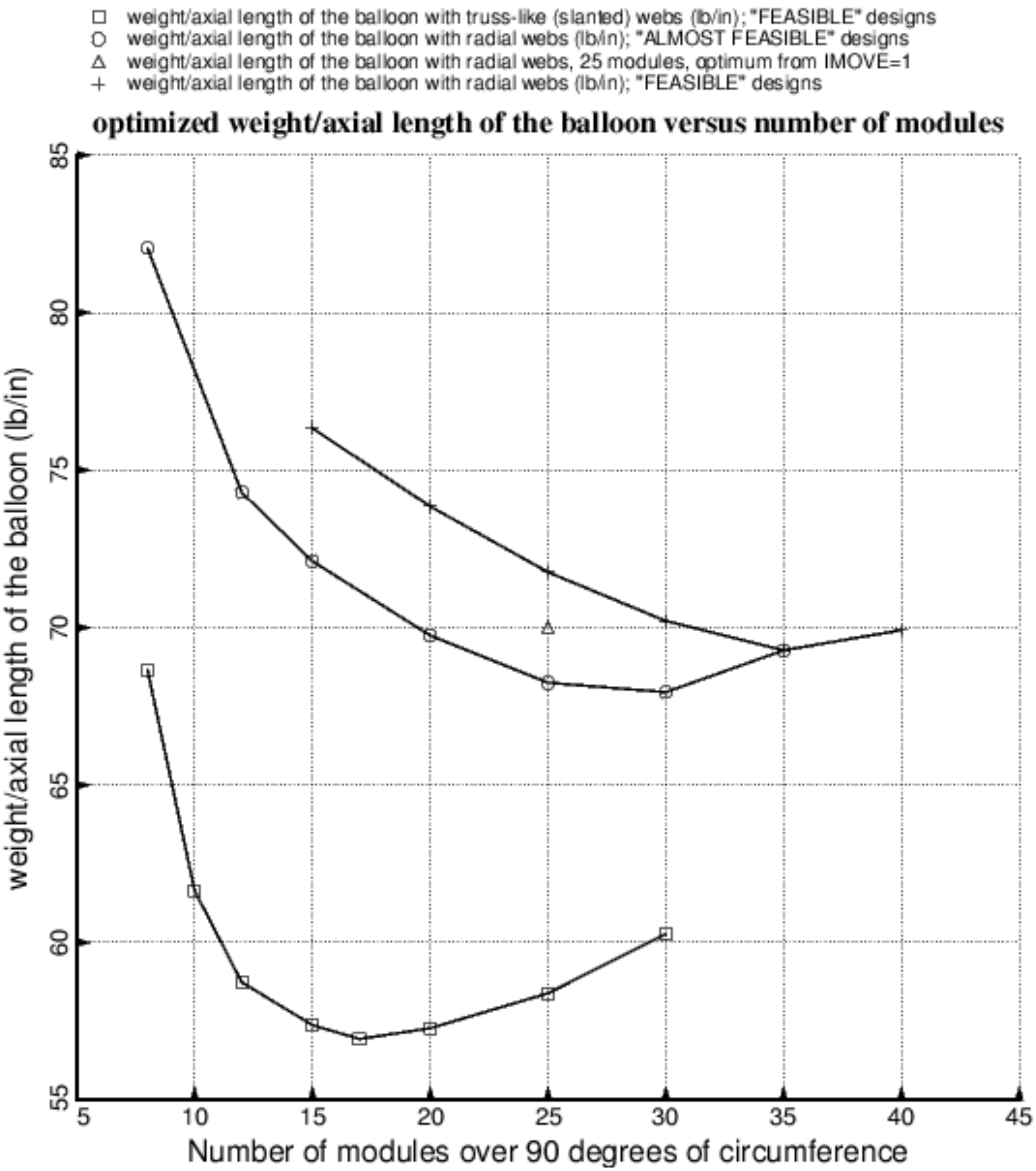

Fig. 25 Optimized weight of the balloons with the truss-like (slanted) webs (trace no. 1) and optimized weight of the balloons with the radial webs (traces 2,3,4) as functions of the number of modules over 90 degrees of circumference of the cylindrical vacuum chamber. The best design of the balloon with the truss-like webs weighs significantly less than the best design of the balloon with the radial webs. The data points in this figure required about 3 weeks of calendar time to produce because of long computer runs, especially for the designs with more than 15 modules. An "ALMOST FEASIBLE" design is a design in which the most critical margin is greater than –0.05 and less than –0.01. A "FEASIBLE" design is a design in which the most critical margin is greater than –0.01.

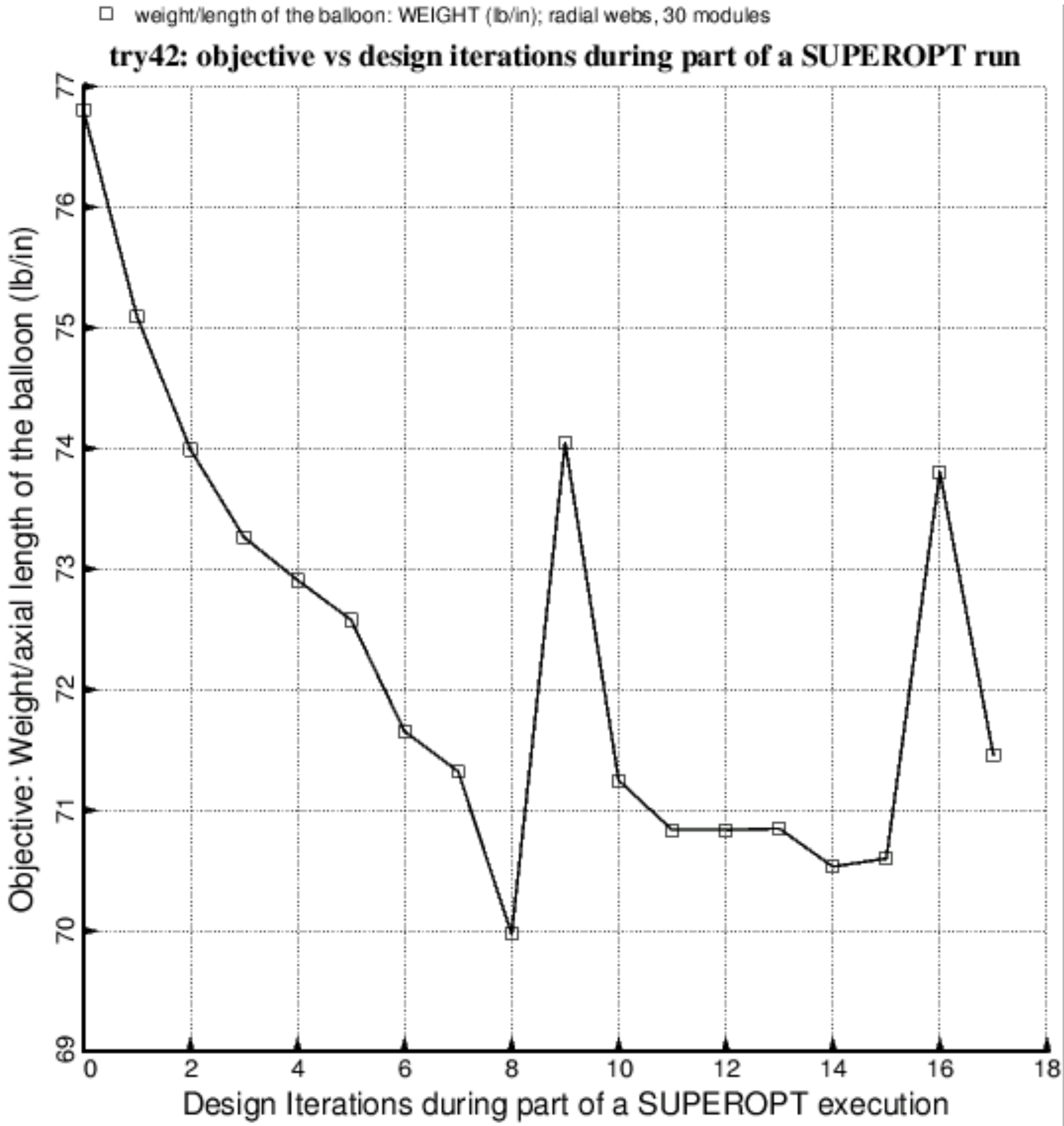

Fig. 26 Optimization of the balloon with radial webs and 30 modules. This execution of SUPEROPT aborted at Design Iteration No. 18 because of failure of convergence of the nonlinear pre-buckling equilibrium solution during Load Step No. 1, for which the applied loads are PINNER, PMIDDL, and DELTAT [the "fixed" (non-eigenvalue) loads]. At the time this run was made SUBROUTINE BEHX1 included only two attempts to solve the nonlinear problem (**Try no. 1** and **Try no. 2** identified in **Item 9** listed in **Section 8**). Introduction of a third attempt, **Try no. 3**, solved the problem.

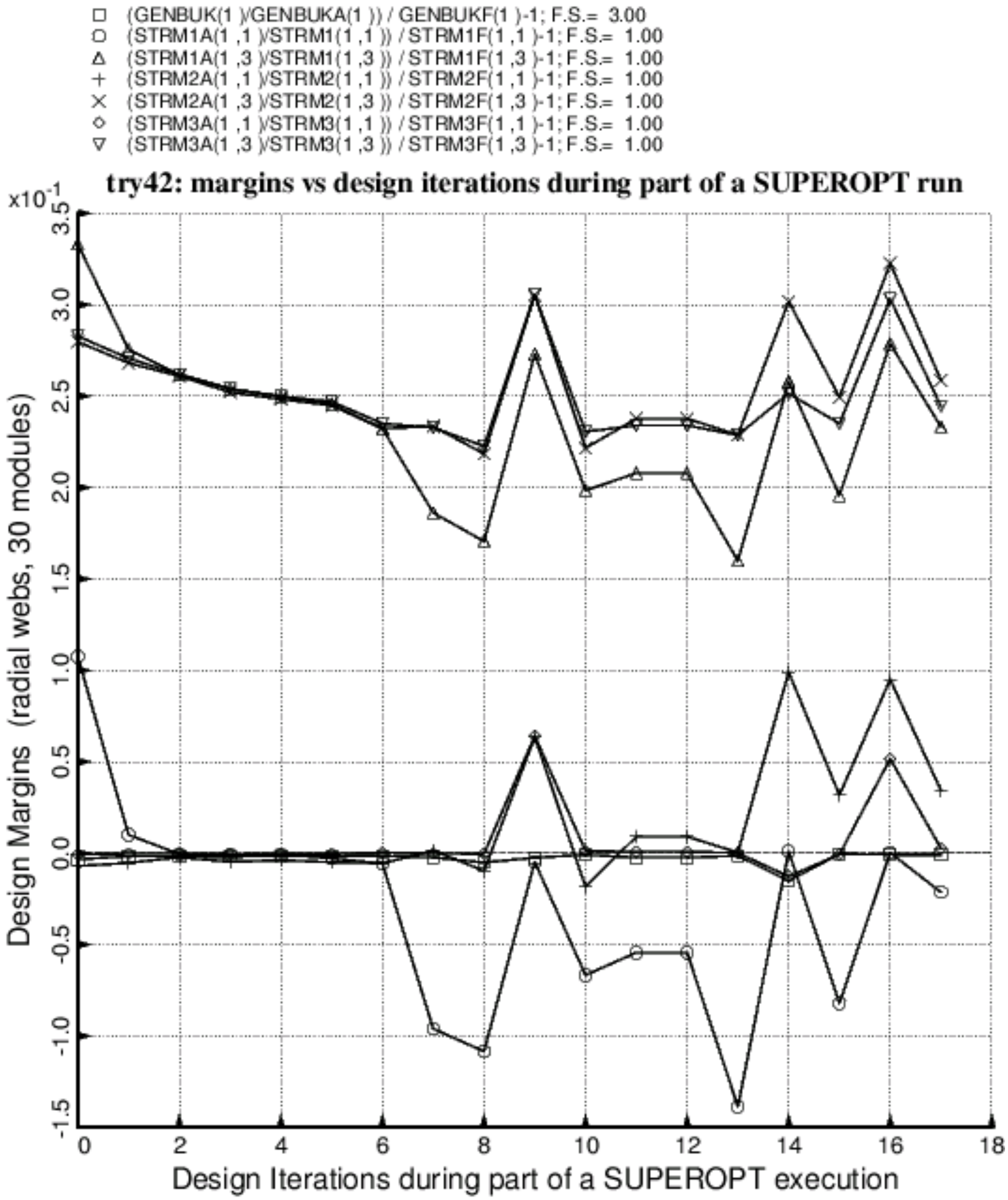

Fig. 27 Optimization of the balloon with radial webs and 30 modules. This execution of SUPEROPT aborted at Design Iteration No. 18 because of failure of convergence of the nonlinear pre-buckling equilibrium solution during Load Step No. 1, for which the applied loads are PINNER, PMIDDL, and DELTAT [the “fixed” (non-eigenvalue) loads]. At the time this run was made SUBROUTINE BEHX1 included only two attempts to solve the nonlinear problem (**Try no. 1** and **Try no. 2** identified in **Item 9** listed in **Section 8**). Introduction of a third attempt, **Try no. 3**, solved the problem.

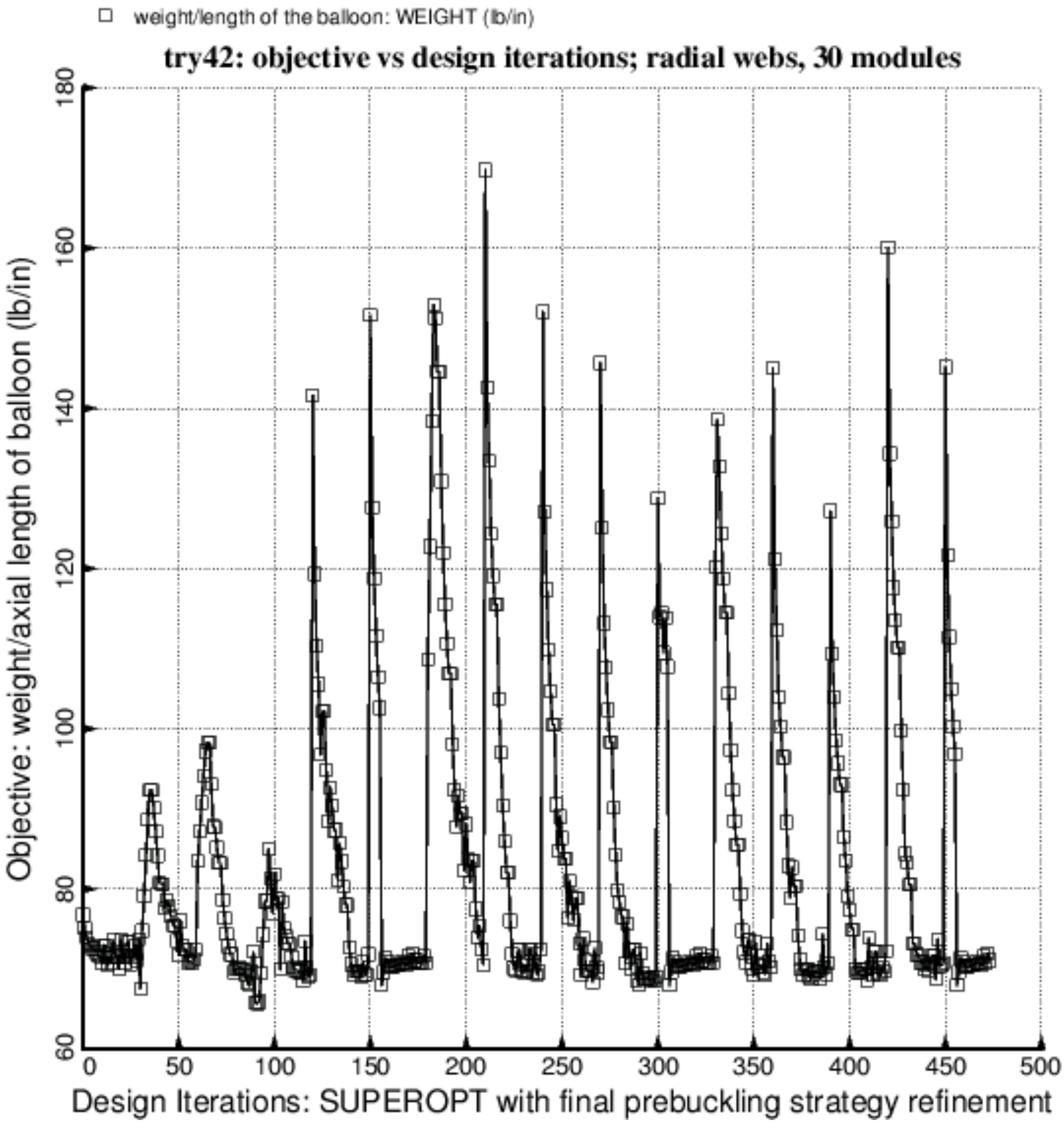

Fig. 27b Optimization of the balloon with radial webs and 30 modules after the introduction into SUBROUTINE BEHX1 of **Try no. 3** in the strategy to solve the nonlinear pre-buckling equilibrium equations. (See **Item 9** listed in **Section 8.**) This execution of SUPEROPT ran to a normal termination at about 470 design iterations. Compare with Fig. 26.

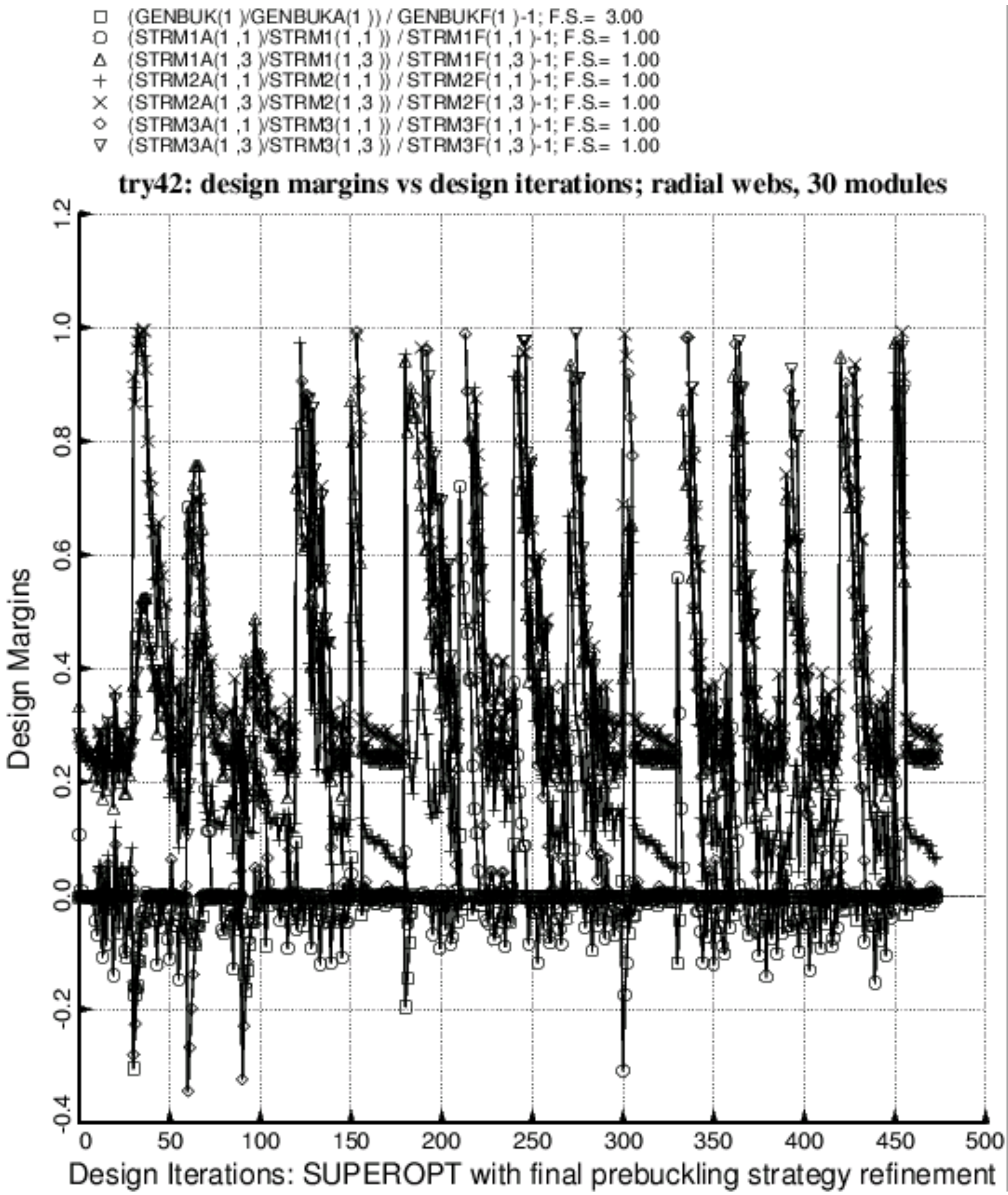

Fig. 27c Optimization of the balloon with radial webs and 30 modules after the introduction into SUBROUTINE BEHX1 of **Try no. 3** in the strategy to solve the nonlinear pre-buckling equilibrium equations. (See **Item 9** listed in **Section 8.**) This execution of SUPEROPT ran to a normal termination at about 470 design iterations. Compare with Fig. 27. Ordinarily one does not bother with plots of design margins subsequent to a completed execution of SUPEROPT because the plot, containing results from about 470 design iterations, is so messy.

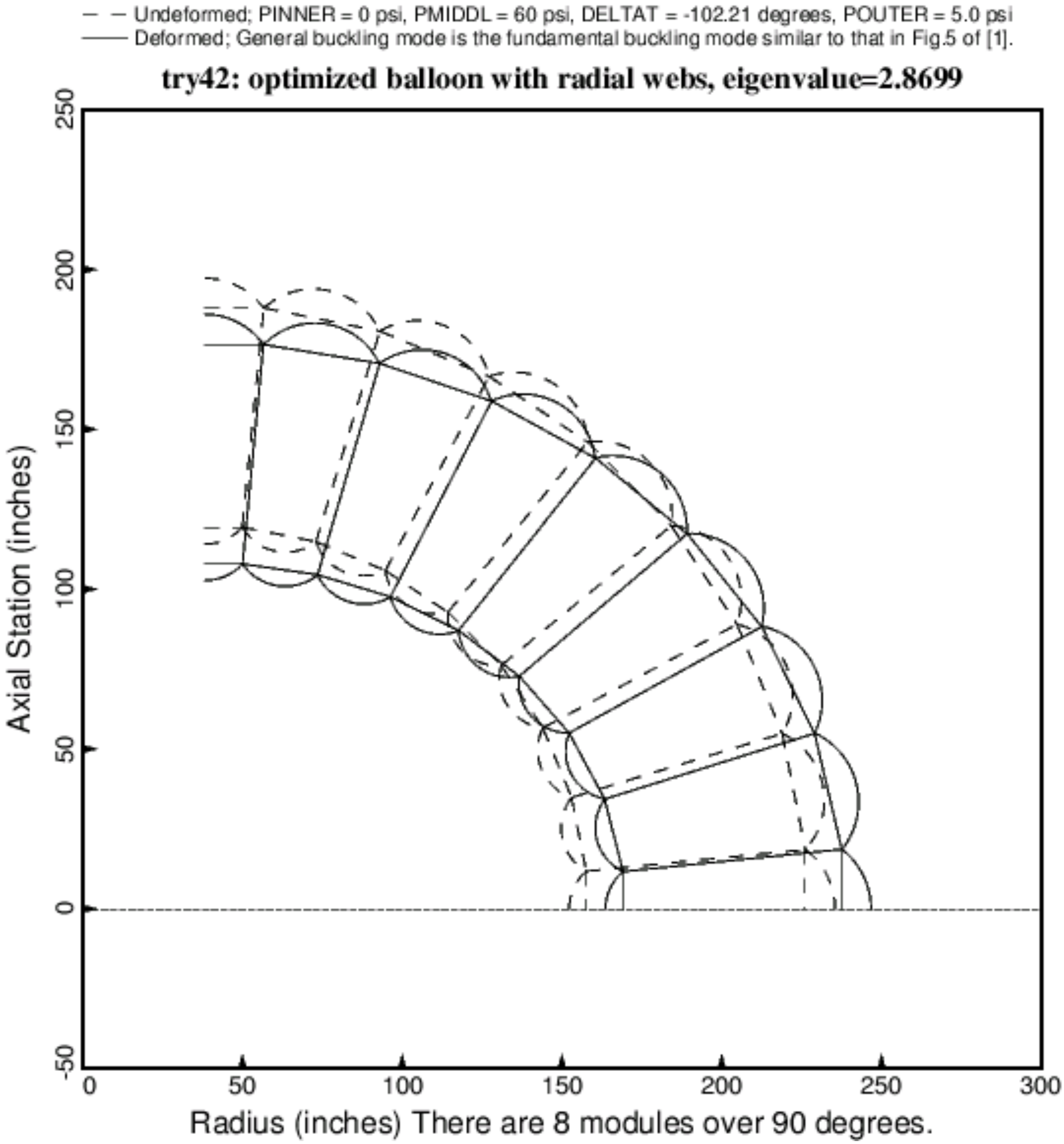

Fig. 28 General buckling of the optimized balloon with radial webs and 8 modules.

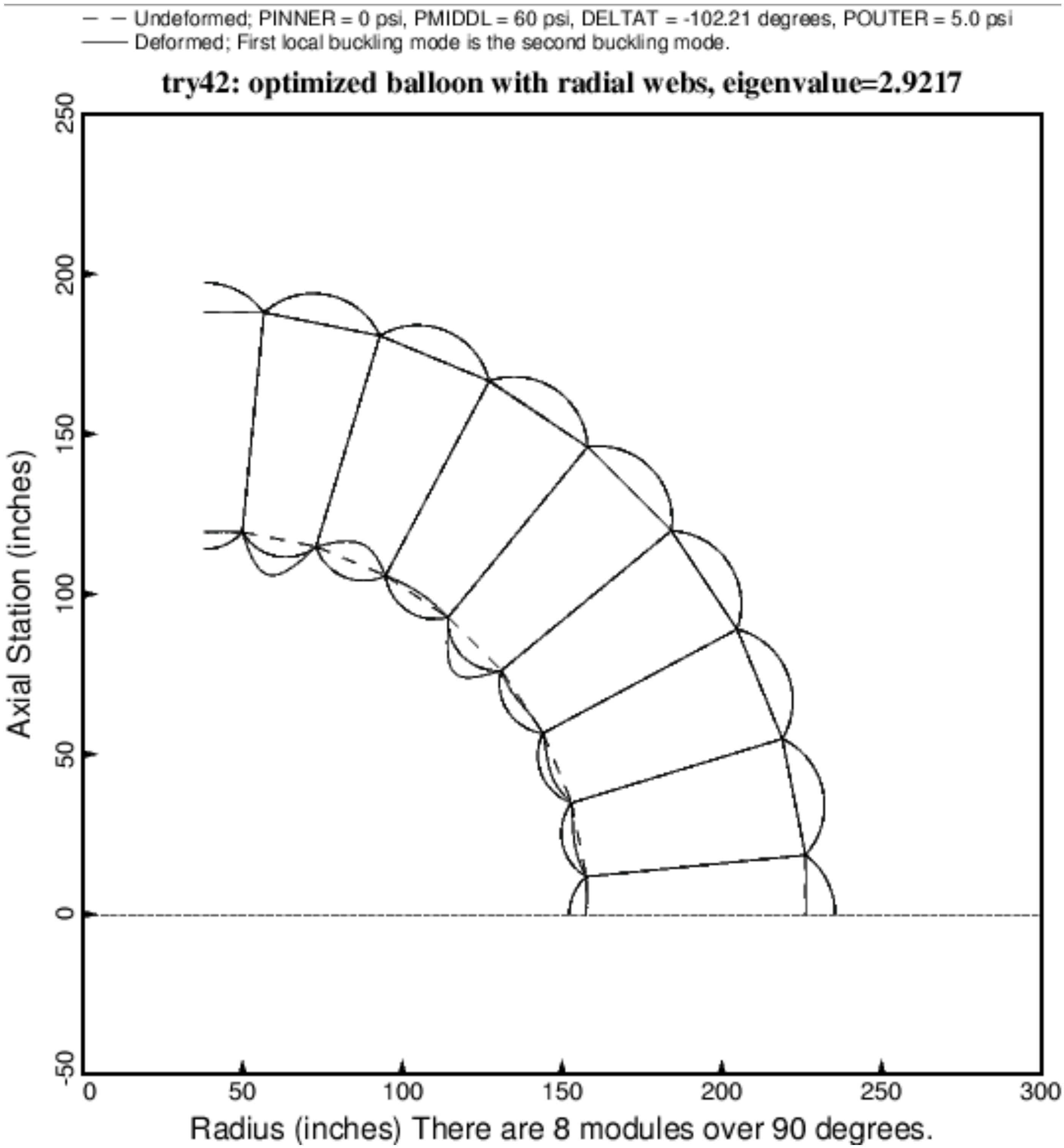

Fig. 29 Local buckling of the optimized balloon with radial webs and 8 modules. This local buckling mode corresponds to eigenvalue no. 2.

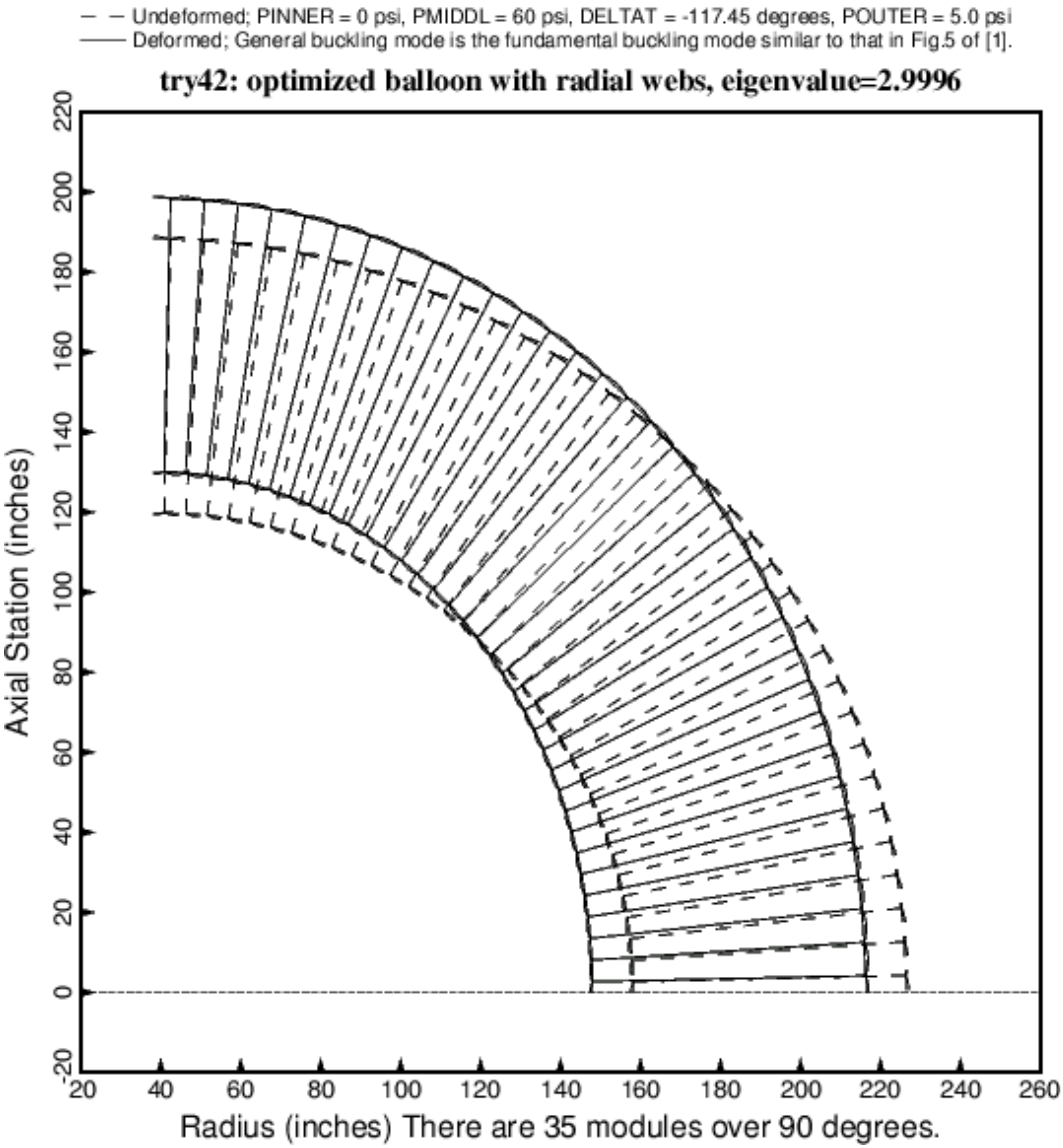

Fig. 30 General buckling of the optimized balloon with radial webs and 35 modules.

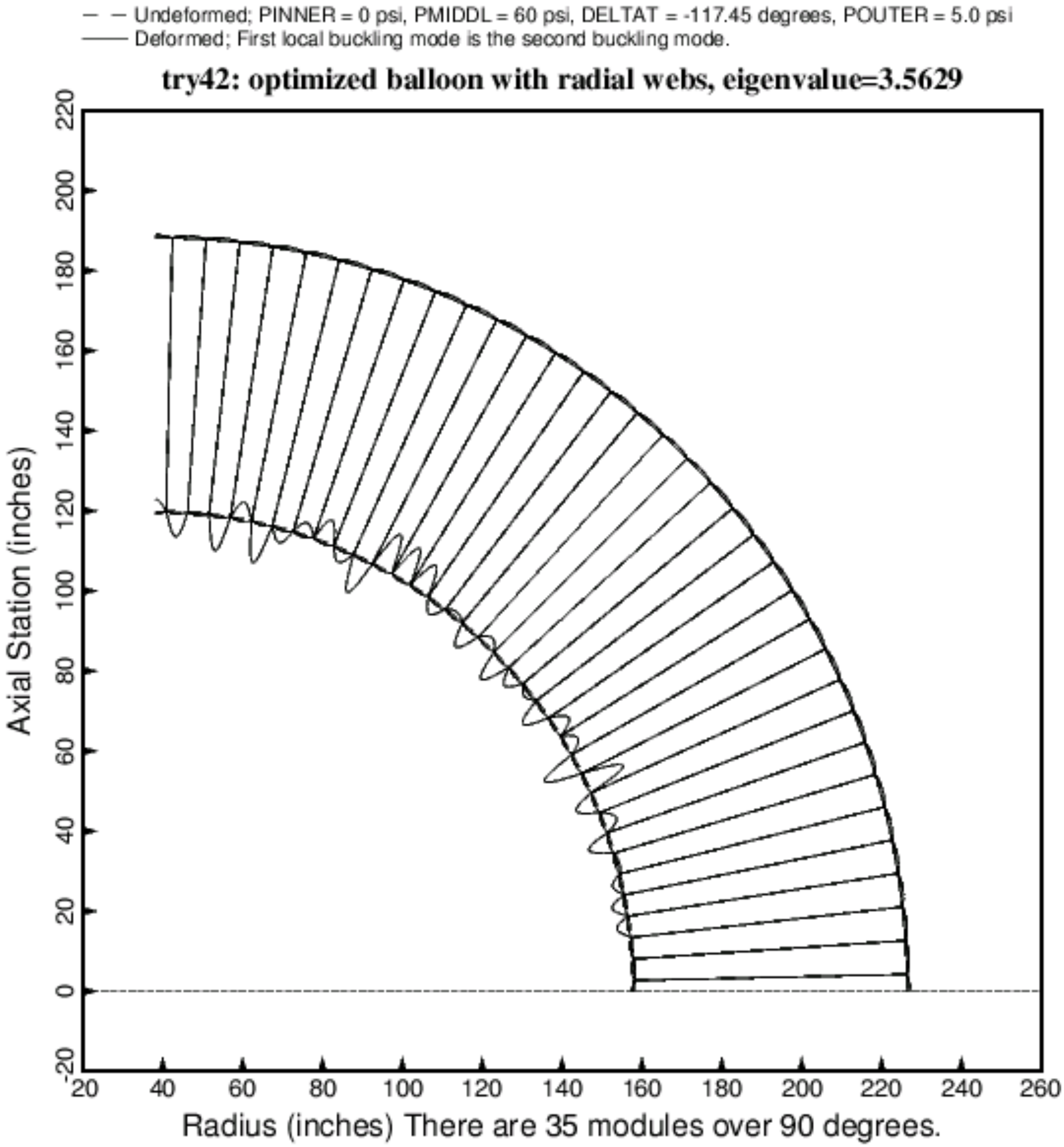

Fig. 31 Local buckling of the optimized balloon with radial webs and 35 modules. This local buckling mode corresponds to eigenvalue no. 2. Eigenvalues 3, 4, 5,,… are all very close to Eigenvalue No. 2 and all of them correspond to buckling of the inner straight segmented membrane of thickness, TFINNR.

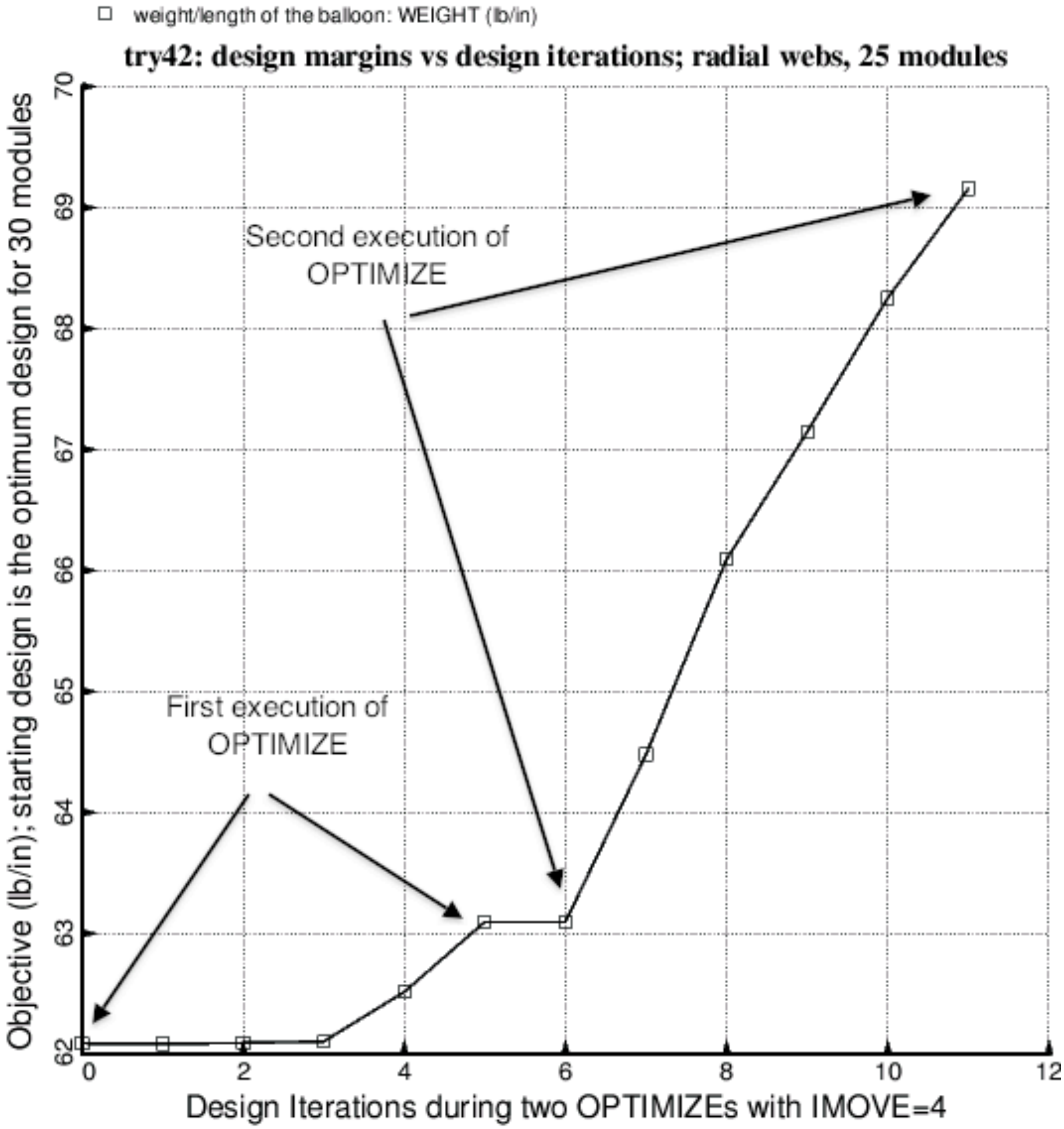

Fig. 32 Optimization of the balloon with the radial webs and 25 modules. The “move limit” index, IMOVE, is set equal to 4, which restricts the change of each decision variable to 2 per cent of its current value during a single optimization cycle. The data points in this plot were obtained via two successive executions of OPTIMIZE by the end user, rather than by a partial execution of SUPEROPT. IMOVE = 4 is more restrictive than IMOVE = 1. IMOVE = 4 is used to close in on a local optimum design in the neighborhood of a previously found optimum obtained with the use of IMOVE = 1. The plots of objective versus design iterations are usually smoother with the use of IMOVE = 4 than with IMOVE = 1, but a less extensive region of design space is explored when IMOVE = 4.

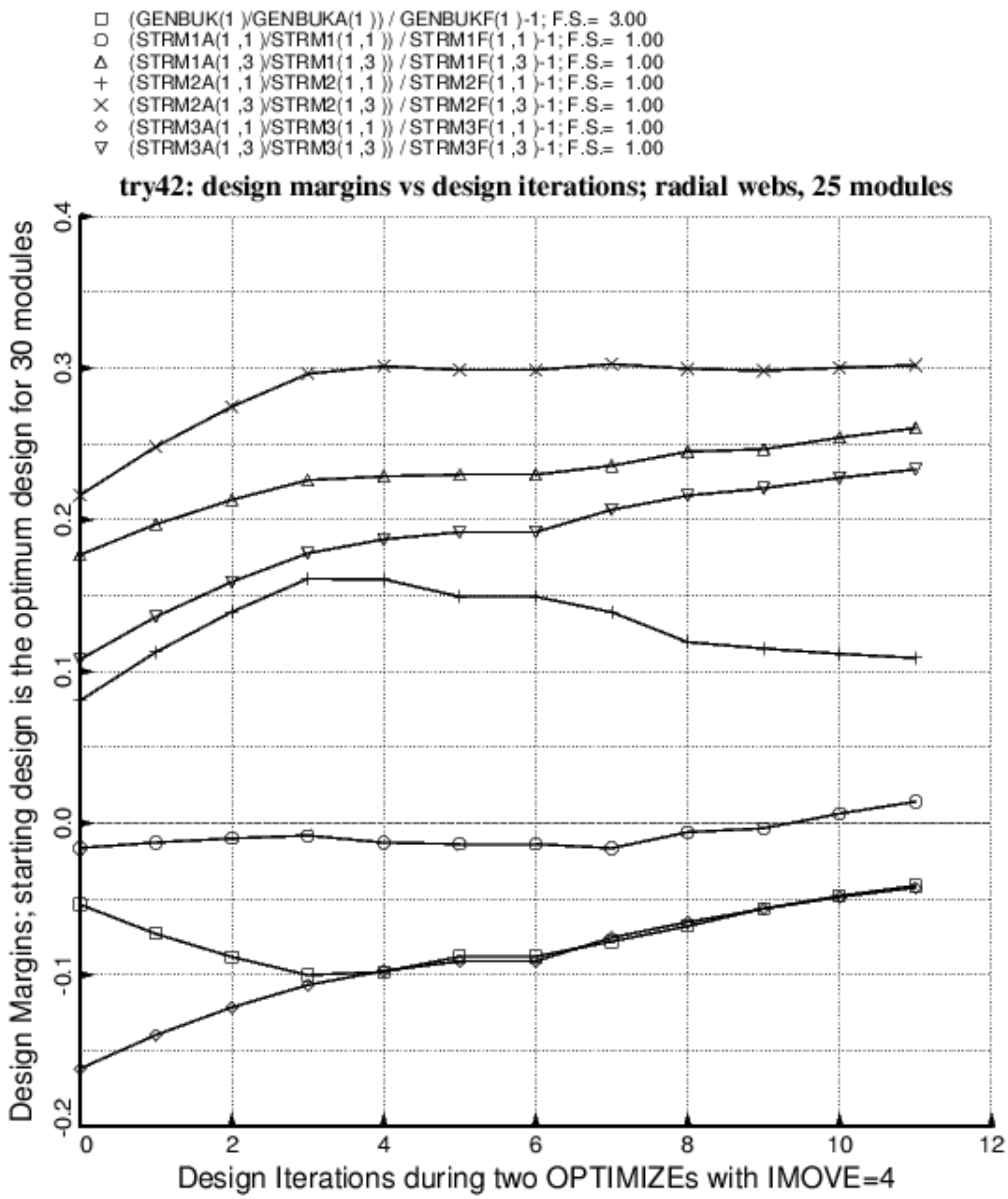

Fig. 33 Optimization of the balloon with the radial webs and 25 modules. The "move limit" index, IMOVE, is set equal to 4, which restricts the change of each decision variable to 2 per cent of its current value during a single optimization cycle. The data points in this plot were obtained via two successive executions of OPTIMIZE by the end user (see the previous figure), rather than by a partial execution of SUPEROPT. IMOVE = 4 is more restrictive than IMOVE = 1. IMOVE = 4 is used to close in on a local optimum design in the neighborhood of a previously found optimum obtained with the use of IMOVE = 1. The plots of design margins versus design iterations are usually smoother with the use of IMOVE = 4 than with IMOVE = 1, but a less extensive region of design space is explored when IMOVE = 4. Compare this figure, generated with IMOVE = 4, with Fig. 27, which was generated from an incomplete SUPEROPT run in which IMOVE=1.

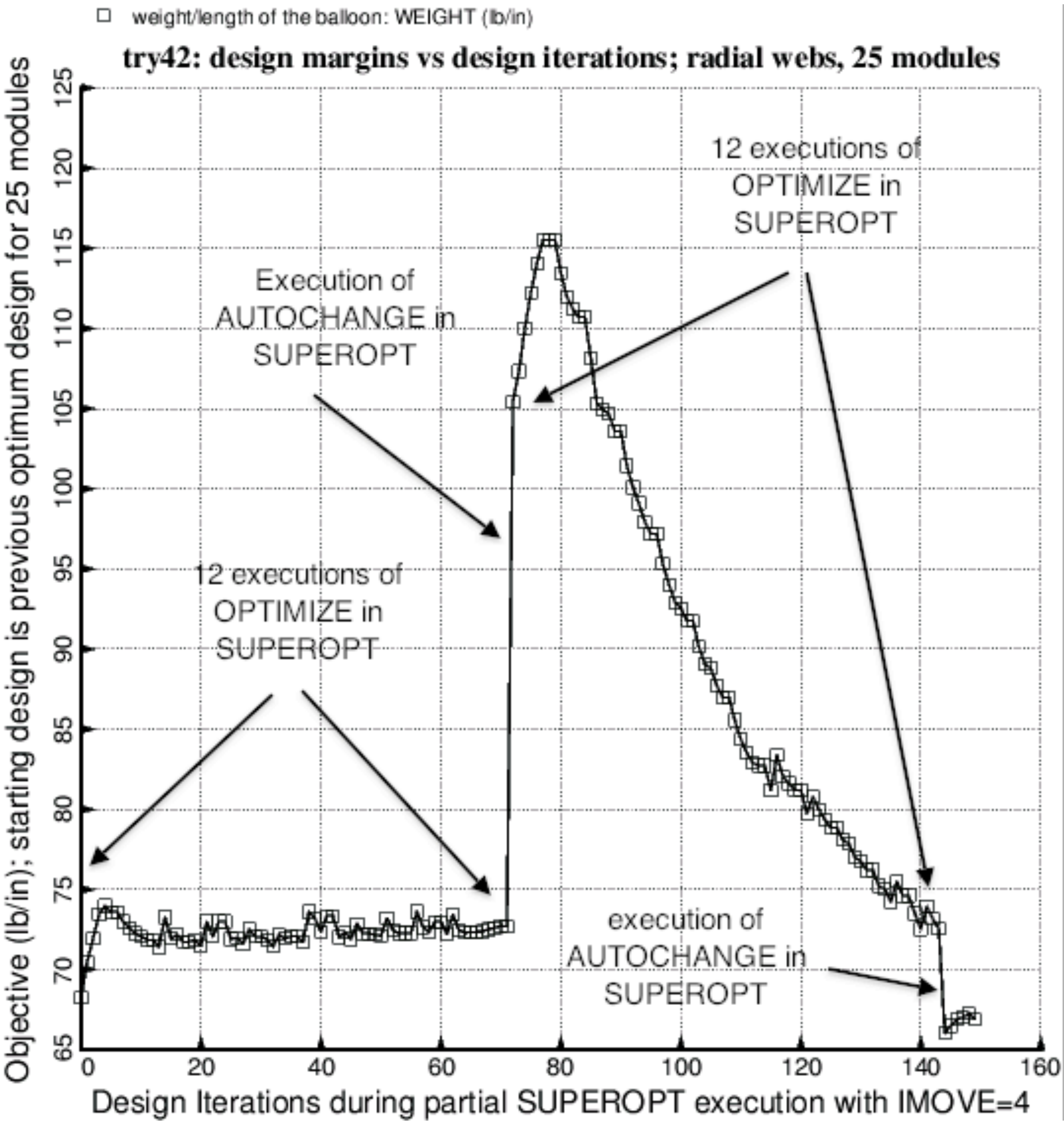

Fig. 34 Results of a SUPEROPT run with IMOVE = 4 and with the end user's specification that there be 12 executions of OPTIMIZE for each execution of AUTOCHANGE in the "SUPEROPT" context. Note that with IMOVE = 4 many executions of OPTIMIZE are required for re-convergence to a local optimum design (see design iterations 73 – 143). Figure 27b, which was generated with IMOVE = 1, demonstrates that fewer executions of OPTIMIZE are require per execution of AUTOCHANGE for re-convergence to local optimum designs. This characteristic enables much more design space to be explored during an execution of SUPEROPT when IMOVE = 1 than is the case when IMOVE = 4. Ordinarily, SUPEROPT should be executed only with IMOVE = 1.

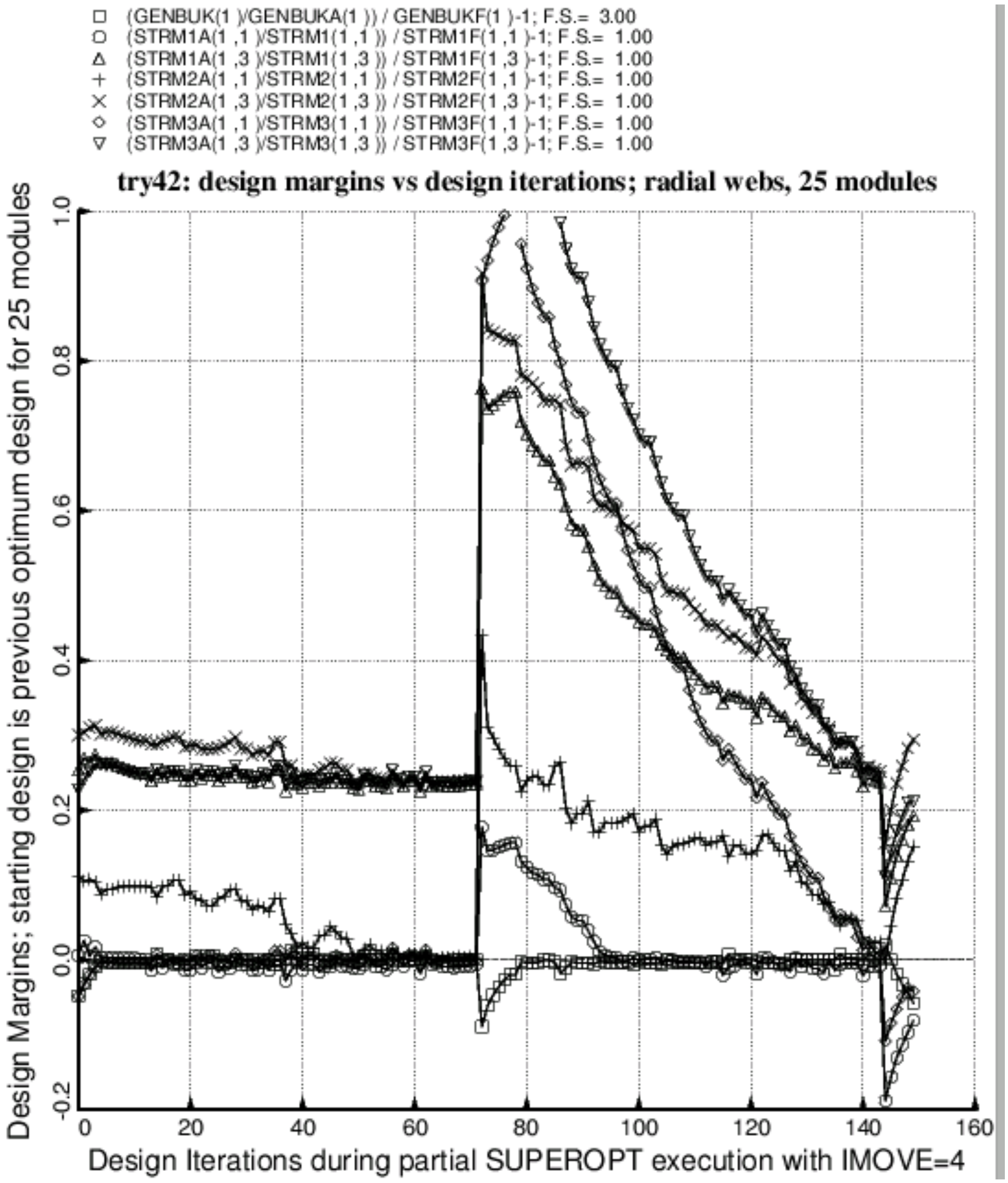

Fig. 35 Results of a SUPEROPT run with IMOVE = 4 and with the end user's specification that there be 12 executions of OPTIMIZE for each execution of AUTOCHANGE in the "SUPEROPT" context. (See the previous figure.) Note that with IMOVE = 4 many executions of OPTIMIZE are required for re-convergence to a local optimum design (see design iterations 73 – 143). Figure 27b, which was generated with IMOVE = 1, demonstrates that fewer executions of OPTIMIZE are require per execution of AUTOCHANGE for re-convergence to local optimum designs. This characteristic enables much more design space to be explored during an execution of SUPEROPT when IMOVE = 1 than is the case when IMOVE = 4. Ordinarily, SUPEROPT should be executed only with IMOVE = 1.